R-08-104

Evaluation and modelling of SWIW tests performed within the SKB site characterisation programme

Rune Nordqvist, Geosigma AB

August 2008

Svensk Kärnbränslehantering AB
Swedish Nuclear Fuel
and Waste Management Co
Box 250, SE-101 24 Stockholm
Tel +46 8 459 84 00

ISSN 1402-3091
SKB Rapport R-08-104

Evaluation and modelling of SWIW tests performed within the SKB site characterisation programme

Rune Nordqvist, Geosigma AB

August 2008

Abstract

In this report, a comprehensive overview of SWIW (Single Well Injection-Withdrawal) tests carried out within the SKB site investigations at Orskarshamn and Forsmark is presented. The purpose of this study is to make a general review and a comparison of performed SWIW tests within the site investigation programmes at the two sites. The study summarises experimental conditions for each test and discusses factors that may influence the experimental results and evaluation of the tests. Further, an extended model evaluation is carried out using a one-dimensional radial flow and transport model with matrix diffusion and matrix sorption. The intended outcome is an improved understanding of various mechanisms that may influence the SWIW test results and also to improve interpretation of the tests.

Six SWIW test at each site have been carried out, generally resulting in high-quality and well documented experimental data with high tracer recovery. The tests have been performed in surface boreholes at repository depth, ranging approximately between 300 to 700 m borehole lengths. In all of the tests, a non-sorbing tracer (Uranine) and one or two sorbing tracers (cesium and rubidium) have been used simultaneously. A general result is that all of the tests demonstrate a very clear and relatively large retardation effect for the sorbing tracers.

Basic initial modelling of the SWIW tests data, using a one-dimensional radial flow model with advection and dispersion, generally resulted in relatively good agreement between model and experimental data. However, a consistent feature of the initial modelling was a discrepancy between model and experimental data in the later parts of the recovery tracer breakthrough curve. It was concluded that this likely was caused by processes occurring in the tested rock formation and therefore an extended model evaluation (presented in this report) including matrix diffusion was carried out on all of the performed tests.

Evaluated retardation factors for the sorbing tracers vary over a wide range. In some cases, differences in retardation properties may be attributed to fracture mineralogy and water chemistry conditions. The extended model evaluation including matrix diffusion resulted in consistently improved fits of the tail of the tracer breakthrough curves, in particular for the non-sorbing tracer Uranine. However, the matrix diffusion effect is considerably larger than would be indicated from laboratory data for matrix porosity and diffusivity.

It is difficult to assess whether there are significant differences between sites regarding retardation, because the number of tests is limited. However, the largest values for the retardation factor are found for Oskarshamn and the smallest value in Forsmark. Moderate values in between are found at each site.

Sammanfattning

I denna rapport presenteras en övergripande sammanfattning av SWIW-tester (Single-Well Injection-Withdrawal) genomförda inom SKB:s undersökningsprogram i Oskarshamn och Forsmark. Syftet med denna studie är en allmän genomgång och jämförelse av samtliga tester inom de båda undersökta områdena. Experimentella förhållanden presenteras och genomlyses för att identifiera potentiella faktorer som kan påverka resultat av testerna. Utöver detta presenteras en utökad modellutvärdering med radiellt flöde och matrisdiffusion.

Sammanlagt har sex SWIW-tester genomförts inom vartdera undersökningsområdet. Generellt sett har experimentdata av god kvalitet erhållits. Testerna har genomförts i ytborrhål på tänkt förvarsdjup, inom ett intervall av ca 300–700 m borrhålslängd. I samtliga tester har ett icke-sorberande (Uranin) och ett eller två sorberande ämnen (cesium/rubidium) injicerats samtidigt. Generellt har en tydlig och relativt stor retardationseffekt av sorberande ämnen påvisats i samtliga genomförda SWIW-tester.

En första basutvärdering av testerna, med hjälp av en endimensionell radiell flödesmodell med advektion, dispersion och jämviktssorption gav relativt god överensstämmelse mellan modell och experiment, för icke-sorberande såväl som sorberande spårämnen. Dock observerades även konsekvent en diskrepans i slutet av genombrottskurvorna, särskilt för det icke-sorberande spårämnet. Efter en genomgång av möjliga effekter till följd av experimentutrustning och/eller genomförande befanns det som mest troligt att svanseffekten beror av processer i bergformationen. Med anledning av detta gjordes en utökad utvärdering inkluderande även matrisdiffusion för samtliga tester.

Skattade retardationsfaktorer för de sorberande ämnena varierar inom ett tämligen stort intervall. I några fall kan skillnaderna sannolikt härledas till skillnader i sprickmineralogi eller vattenkemiska förhållanden. Modellansatsen med matrisdiffusion resulterade allmänt i förbättrad överensstämmelse mellan modell och experimentdata, särskilt för det icke-sorberande ämnet (Uranin). Dock är den erforderliga matrisdiffusionseffekten väsentligt större an vad som motsvaras av laboratoriedata.

Det är svårt att dra någon generell slutsats om signifikanta skillnader beträffande retardation mellan platserna då antalet genomförda tester är relativt begränsat. Dock finner man de största retardationseffekterna i SWIW-tester från Oskarshamn, medan det lägsta värdet på retardationsfaktorn har erhållits från ett av testerna i Forsmark.

Contents

1 Introduction

A number of SWIW (Single Well Injection-Withdrawal) tests have been carried out within the SKB site characterisation programmes at Oskarshamn and Forsmark. The SWIW tests have generally resulted in high-quality experimental data. All of the performed tests have been subject to a basic model evaluation, assuming homogenous radial flow and transport with advection, dispersion and linear equilibrium sorption. This basic model evaluation has been carried out using a best-fit procedure with simultaneous fitting of non-sorbing and sorbing tracers.

The results from the evaluation of the various SWIW tests have generally showed relatively good agreement between model and experimental data. However, a re-occurring feature of the evaluation results is that, although the ascending part as well most of the descending part can be fitted well with the simple model employed, the tail of the tracer breakthrough curves can in most cases not be fitted.

The purpose of this study is to make a general review and comparison of performed SWIW tests within the site investigation programmes at the two sites. The study summarises experimental conditions for each test and discusses factors that may influence the experimental results and evaluation of the tests. Further, an extended model evaluation is carried out using a one-dimensional radial flow and transport model with matrix diffusion and matrix sorption. The intended outcome is an improved understanding of various mechanisms that may influence the SWIW test results and also to improve interpretation of the tests.

2 Background

2.1 Outline of a SWIW test

A SWIW test may consist of all or some of the following phases:

1. Injection of fluid to establish steady state hydraulic conditions.
2. Injection of one or more tracers.
3. Injection of a chaser fluid after tracer injection is stopped, possibly also label the chaser fluid with a different tracer.
4. Waiting phase.
5. Recovery phase.

The waiting phase is sometimes also called the shut-in period or resting period.

The tracer breakthrough data that is eventually used for evaluation is obtained from the recovery phase. The injection of chaser fluid has the effect of pushing the tracer out as a "ring" in the formation surrounding the tested section. An advantage of this is that when the tracer is pumped back both the ascending as well as the descending parts in the recovery breakthrough curve are obtained. During the waiting phase there is no injection or withdrawal of fluid. The purpose of this phase is often to increase the time available for time-dependent transport-processes so that these may be more easily evaluated from the resulting breakthrough curve. A schematic example of a resulting breakthrough curve during a SWIW test is shown in Figure 2-1.

The design of a successful SWIW test requires prior determination of injection and withdrawal flow rates, duration of tracer injection, duration of the various experimental phases, selection of tracers and tracer injection concentrations.

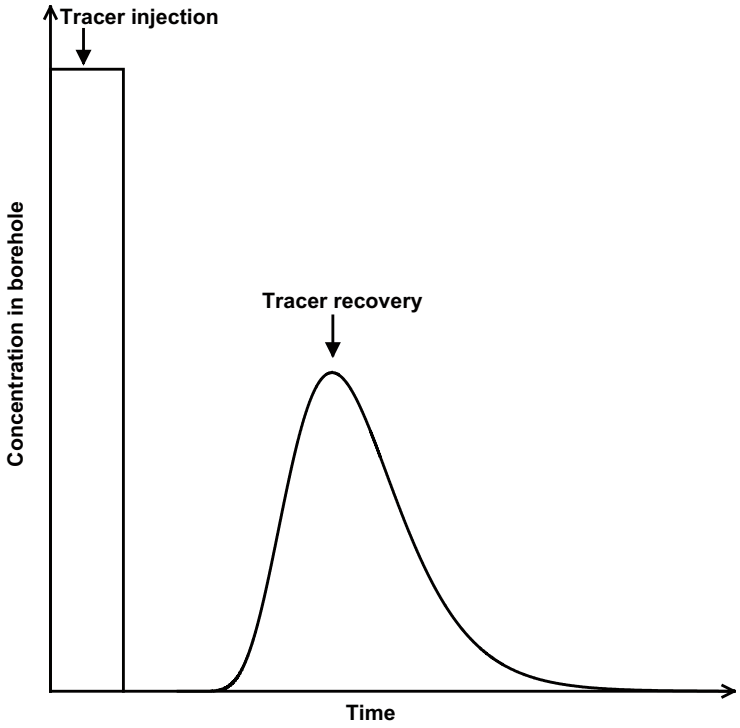

Figure 2-1. *Schematic tracer concentration sequence during a SWIW test.*

2.2 Overview of experimental procedures for SWIW tests within the site investigations

2.2.1 Equipment

The SWIW (Single Well Injection Withdrawal) test equipment constitutes a complement to the borehole dilution probe /Gustafsson 2002/, making it possible to carry out a SWIW test in the same test section as the dilution measurement, see Figure 2-2. Measurements can be made in boreholes with 56 mm or 76–77 mm diameter and the test section length can be 1, 2, 3, 4 or 5 m with a special packer/dummy system for 76–77 mm boreholes. The equipment is primarily designed for measurements in the depth interval of 300–700 m borehole length. However, measurements can be carried out at shallower depths as well as at depths larger than 700 m. The possibility to carry out a SWIW test much depends on the hydraulic transmissivity and natural

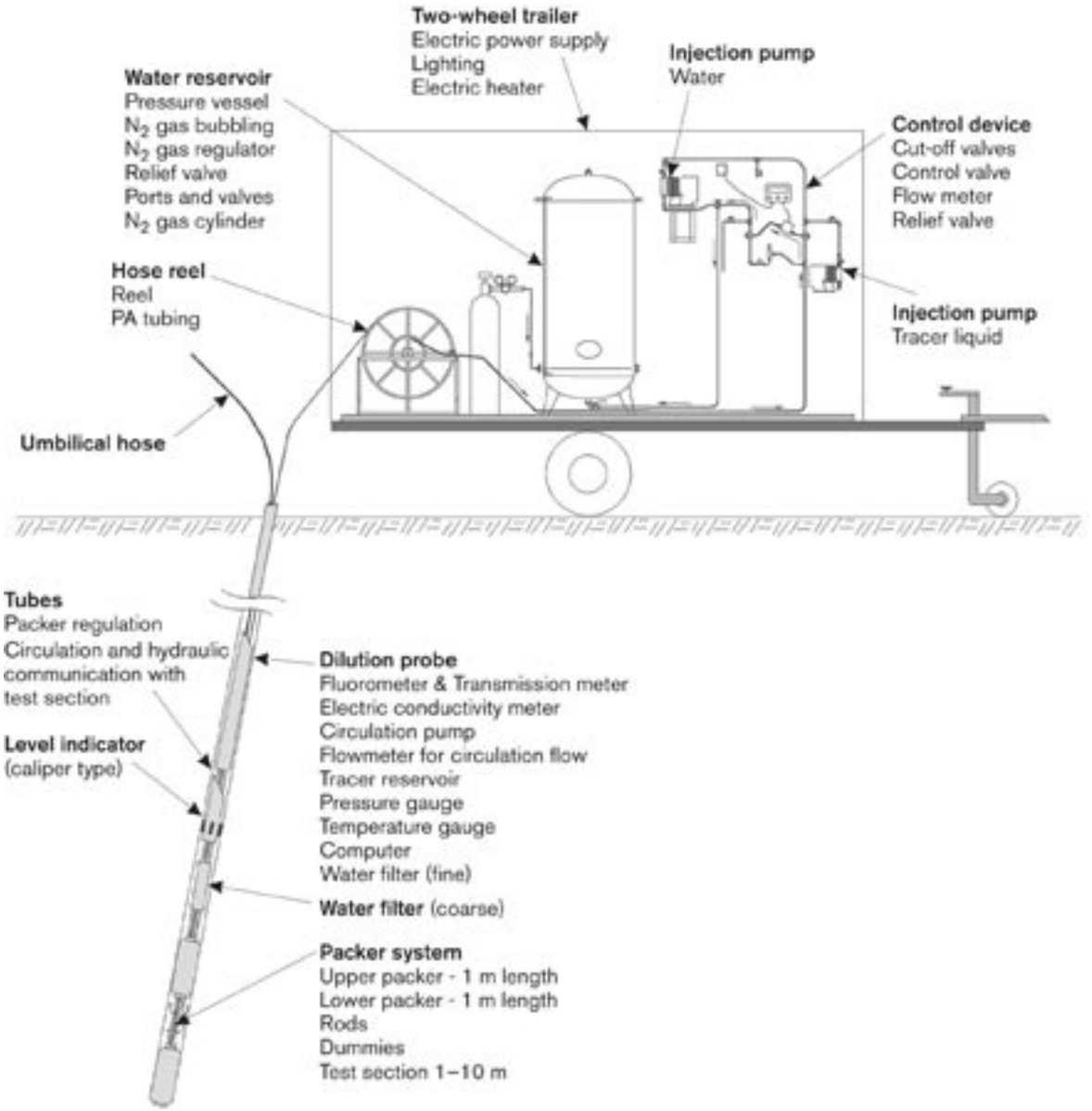

Figure 2-2. *SWIW test equipment, connected to the borehole dilution probe /from Gustafsson et al. 2005/.*

groundwater flow in the investigated test section, and frictional loss in the tubing at tracer withdrawal pumping (recovery phase). Besides the dilution probe, the main parts of the SWIW test equipment are:

- Polyamide tubing (6 mm inner diameter) constituting the hydraulic connection between SWIW test equipment at the ground surface and the dilution probe in the borehole.
- Air tight pressure vessel for storage of groundwater under anoxic and pressurised conditions, i.e. N_2-athmosphere.
- Control system for injection of tracer solution and groundwater (chaser fluid).
- Injection pumps for tracer solution and groundwater.

2.2.2 Measurement range and accuracy

The result of a SWIW test depends on the accuracy in the determination of the tracer concentration in injection solutions and withdrawn water. The result also depends on the accuracy in the volume of injection solution and volumes of injected and withdrawn water. For non-sorbing dye tracers (e.g. Uranine), the tracer concentration in collected water samples can be analysed with a resolution of 10 µg/l in the range of 0.0–4.0 mg/l. The accuracy is within ± 5%. The volume of injected tracer solution can be determined within ± 0.1% and the volume of injected and withdrawn water determined within 5%.

2.2.3 Experimental procedure

The SWIW tests within the site investigation programmes are generally carried out according to the following procedure. The equipment is lowered to the correct borehole length where background values of Uranine and supporting parameters, pressure and temperature, are measured and logged. Then, after inflation of packers and pressure stabilization, the circulation pump in the dilution probe is used to pump groundwater from the test section to the air-tight vessel at the ground surface. Water samples are also taken for analysis of tracer background concentrations. After pressure recovery following the pumping, pre-injection of the native groundwater, in order to obtain steady state flow conditions, is started. Thereafter groundwater spiked with the tracer(s) is injected. As a final injection phase, injection of native groundwater to push the tracers out into the fracture/fracture zone is carried out. The withdrawal phase is then started by pumping water to the ground surface. An automatic sampler at the ground surface is employed to take water samples for analysis of tracer content in the withdrawn water.

2.3 Overview of performed tests within the site investigation programmes

SWIW tests have been carried in the following borehole sections, in chronological order:

- KSH02, 422.3–423.3 m September 2004
- KSH02, 576–579.8 m September–October 2004
- KFM03A, 643.5–644.5 m January 2005
- KFM02A, 414.7–417.7 m February–March, 2005
- KLX03, 740.4–744.4 m September–October 2005
- KFM08A, 410.5–413.5 m December 2005
- KFM04A, 417.0–422.0 m February–March 2006

- KLX18A, 473.3–476.3 m September–November 2006
- KFM01D, 377.4–378.4 m December 2006–March 2007
- KFM01D, 431.0–432.0 m December 2006–March 2007
- KLX11A, 516.5–519.5 m March–July 2007
- KLX11A, 598.0–599.0 m March–July 2007

Prior to these tests, a Site Acceptance Test (SAT) was performed in borehole KLX02 /Gustafsson et al. 2004/.

In the listed tests above, a non-sorbing tracer was injected together with at least one sorbing tracer. In all of the tests, Uranine (non-sorbing) and cesium (strongly sorbing) were injected. In addition, rubidium was injected as a second sorbing tracer in all tests except in KSH02, KFM02A and KFM03A.

The test results along with a basic evaluation of data are presented in the following reports:

- KSH02: /Gustafsson and Nordqvist 2005/.
- KFM02A and KFM03A: /Gustafsson et al. 2005/.
- KLX03: /Gustafsson et al. 2006a/.
- KFM08A: /Gustafsson et al. 2006b/.
- KFM04A: /Gustafsson et al. 2006c/.
- KLX18A: /Thur et al. 2007a/.
- KFM01D: /Thur et al. 2007b/.
- KLX11A: /Thur et al. 2007c/.

3 Overview of experimental results

3.1 Experimental conditions

The SWIW tests within the site investigation programmes were carried out at expected repository depths, between 300–700 m. The transmissivity of the tested features ranged approximately between 10^{-8} to 10^{-6} m^2/s, and tested features comprised single fractures as well as minor fracture zones. The tests were typically carried out with a 1–2 hour long tracer injection period followed by a 10–20 hour long chaser injection period. Total injected water volumes ranged approximately between 100 to 340 L. The length of the test sections varied between one and five metres. The section length was for each test selected so that all of the flowing features at that depth would be between the packers, in order to avoid hydraulic shortcuts to the borehole outside the packer interval.

A summary of some of the more relevant experimental conditions for the SWIW tests is presented in Table 3-1. Total injected water volume determines how far into the surrounding formation the tracer travels, while the duration of the various injection phases gives a measure of the time available for possible time-dependent transport processes. The waiting phase durations are shown separately although waiting phases were generally not used. However, for the test in KSH02, section 422.3–423.3 m, most of the chaser injection period consisted of a pump repair period with only a small outflow from the section (as a result of released packers).

Table 3-1. Basic features of the SWIW tests performed within the site investigations.

Borehole	Section (m)	Depth (m.a.s.l.)	T (m^2/s)	# of fractures	Total injected water volume (L)	Injection+chaser time duration (hours)	Waiting phase duration (hours)
KSH02	422.3–423.3	–417	1.0E–06	1	204	61.5*	2.8
KSH02	576.9–579.8	–571	5.2E–07	Fracture zone; 3–4 flowing fractures	175	15.3	0
KLX03	740.4–744.4	–701	4.0E–06	Fracture zone; 5–10 flowing fractures	336	15.3	0.7
KLX18A	473.3–476.3	–468	4.3E–08	Fracture zone; 3–4 flowing fractures	122	50	0
KLX11A	516.5–519.5	–448	3.4E–06	2	116	6.4	0
KLX11A	598.0–599.0	–515	1.4E–07	Fracture zone; 2 flowing fractures	113	11.7	0
KFM02A	414.7–417.7	–407	9.5E–07	Fracture zone; 1–3 flowing fractures	201	15.2	0
KFM03A	643.5–644.5	–633	2.5E–06	Minor fracture zone with 3 flowing fractures	127	12.7	1.4
KFM08A	410.5–413.5	–340	1.0E–08	3	172	75.2	0
KFM04A	417.0–422.0	–355	8.9E–09	1–2 open fractures in a sealed network of fracture zone	177	75.3	0.1
KFM01D	377.4–378.4	–300	3.2E–07	1	113	8.3	0.1
KFM01D	431.0–432.0	–342	1.0E–06	1	112	8.6	0.5

* Most of the chaser injection phase in KSH02, 422.3–423.3 m, took place during pump repair. During this, packers were released which resulted in a small outflow of water from the section.

The total injected volumes vary somewhat among the performed tests. This variation is partly a reflection of the transmissivity of the section and the available experimental time frame, which depends on other planned activities at the site. The total injected water volume determines the magnitude of the distance a non-sorbing tracer travels out into the formation, but cannot be determined because the volume through which the injected water travels is unknown. The radial advective travel distance, r_{adv}, in a single fracture is given by:

$$r_{adv} = \sqrt{\frac{V_{inj}}{\pi\delta} + r_w^2} \qquad (3\text{-}1)$$

where V_{inj} is the total injected water volume [L^3], δ is the equivalent fracture aperture [L] and r_w is the borehole radius [L].

Figure 3-1 shows a plot of plausible travel distances for varying values of fracture aperture calculated from equation 3-1, assuming a single fracture with parallel fracture walls, based on the largest injected volume (KLX03, 740.4–744.4 m) and the smallest injected volume (KFM01D, 431.0–432.0 m), see Table 3-1. It is difficult to narrow down this estimate of the radial travel distance further, because there is no direct independent information about fracture volume. However, a reasonable overall estimate of the magnitude of the radial travel distances in the performed SWIW test may be in the range of 5–20 m.

3.2 Rock characteristics and water chemistry

Selected rock characteristics, obtained from the SICADA database, for the SWIW test sections are listed in Table 3-2. Such information provides useful background information when assessing possible differences in the experimental outcomes among the various SWIW tests. Table 3-2 primarily only lists data for the fractures classified as "certain" in the SICADA data base.

Table 3-2 shows that calcite and chlorite are commonly occurring as dominating fracture minerals in open fractures. An interesting exception is that no fracture minerals are found in the tested section in KFM02A. Alteration states vary from fresh to highly altered.

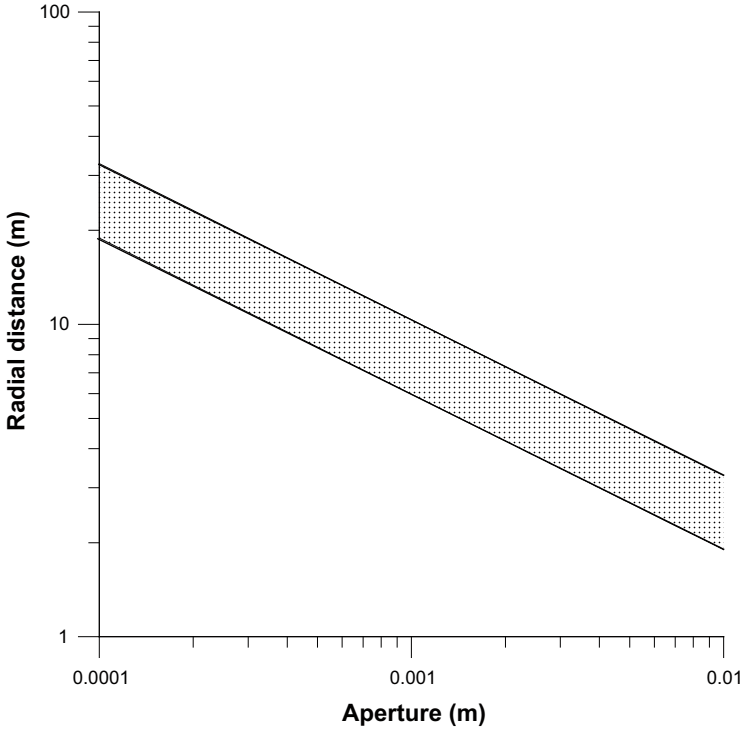

Figure 3-1. *Illustration of plausible radial travel distances for varying apertures based on the largest (upper line, 336 L) and smallest (lower line, 112 L) total injected water volume.*

Table 3-2. Selected rock characteristics for the SWIW test borehole sections.

Borehole	Section (m)	Rock type	# of certain open fractures	Fracture minerals in open fractures	Alteration
KSH02	422.3–423.3	Fine-grained dioritoid (Metavolcanite, vulcanite)	1	Calcite	Moderately altered
KSH02	576.9–579.8	Granite, fine-to medium grained	3	Calcite, chlorite	Slightly altered
KLX03	740.4–744.4	Fine-grained diorite gabbro	3	Chlorite, clay minerals	Slightly altered
KLX18A	473.3–476.3	Granite to quartz monzodiorite, generally porphyric	3 probable	Calcite, chlorite	Fresh (2), Slightly altered (1)
KLX11A	516.5–519.5	Quartz monzonite to monzodiorite	1	Chlorite	Slightly altered
KLX11A	598.0–599.0	Quartz monzodiorite	7 possible	Calcite, chlorite	Slightly altered
KFM02A	414.7–417.7	Granite to granodiorite, metamorphic, medium-grained	6	No minerals	Slightly altered
KFM03A	643.5–644.5	Granite to granodiorite, metamorphic, medium-grained	3	Clay, hematite, chlorite, calcite	Highly altered
KFM08A	410.5–413.5	Granite to granodiorite, metamorphic, medium-grained	1	Chlorite, clay, calcite	Fresh
KFM04A	417.0–422.0	Pegmatite/Granite to granodiorite, metamorphic, medium-grained	7	Zeolites, calcite, chlorite, quartz	Fresh
KFM01D	377.4–378.4	Fine- to finely medium-grained metagranite-granodiorite	1	Chlorite	Slightly altered
KFM01D	431.0–432.0	Fine- to finely medium-grained metagranite-granodiorite	1	Chlorite, calcite	Slightly altered

Selected water chemistry data are presented in Table 3-3, where chloride concentration and electric conductivity for each test section is shown. The chemistry data in Table 3-3 is obtained from water sampling in direct connection with the SWIW test. The table shows that most of the tested sections have water of relatively high salinity. The only section with fresh-water chloride content is KLX11A, section 516.5–519.5.

Table 3-3. Selected water chemistry data from the SWIW test borehole sections.

Borehole	Section (m)	Chloride (mg/L)	Electric conductivity (mS/m)
KSH02	422.3–423.3	8,050	2,100
KSH02	576.9–579.8	5,600	1,570
KLX03	740.4–744.4	1,090	389
KLX18A	473.3–476.3	2,000	611
KLX11A	516.5–519.5	89	68
KLX11A	598.0–599.0	1,040	1,040
KFM02A	414.7–417.7	5,190	1,480
KFM03A	643.5–644.5	5,240	1,540
KFM08A	410.5–413.5	4,700	1,300
KFM04A	417.0–422.0	6,300	1,560
KFM01D	377.4–378.4	4,000	1,060
KFM01D	431.0–432.0	3,700	1,100

3.3 Experimental results

The primary experimental result from the SWIW tests are tracer breakthrough curves from the recovery phase. Measurements are made on samples taken at the ground surface.

Tracer breakthrough curves for all performed SWIW tests within the site investigation programme are shown in Figure 3-2. The breakthrough curves are plotted with normalised concentrations against elapsed time from start of injection. The concentration is normalised by dividing with total injected mass, thereby the breakthrough curves from different tracers can be directly compared for each test. The times are corrected for residence times in the tubing during the injection and recovery phases, respectively.

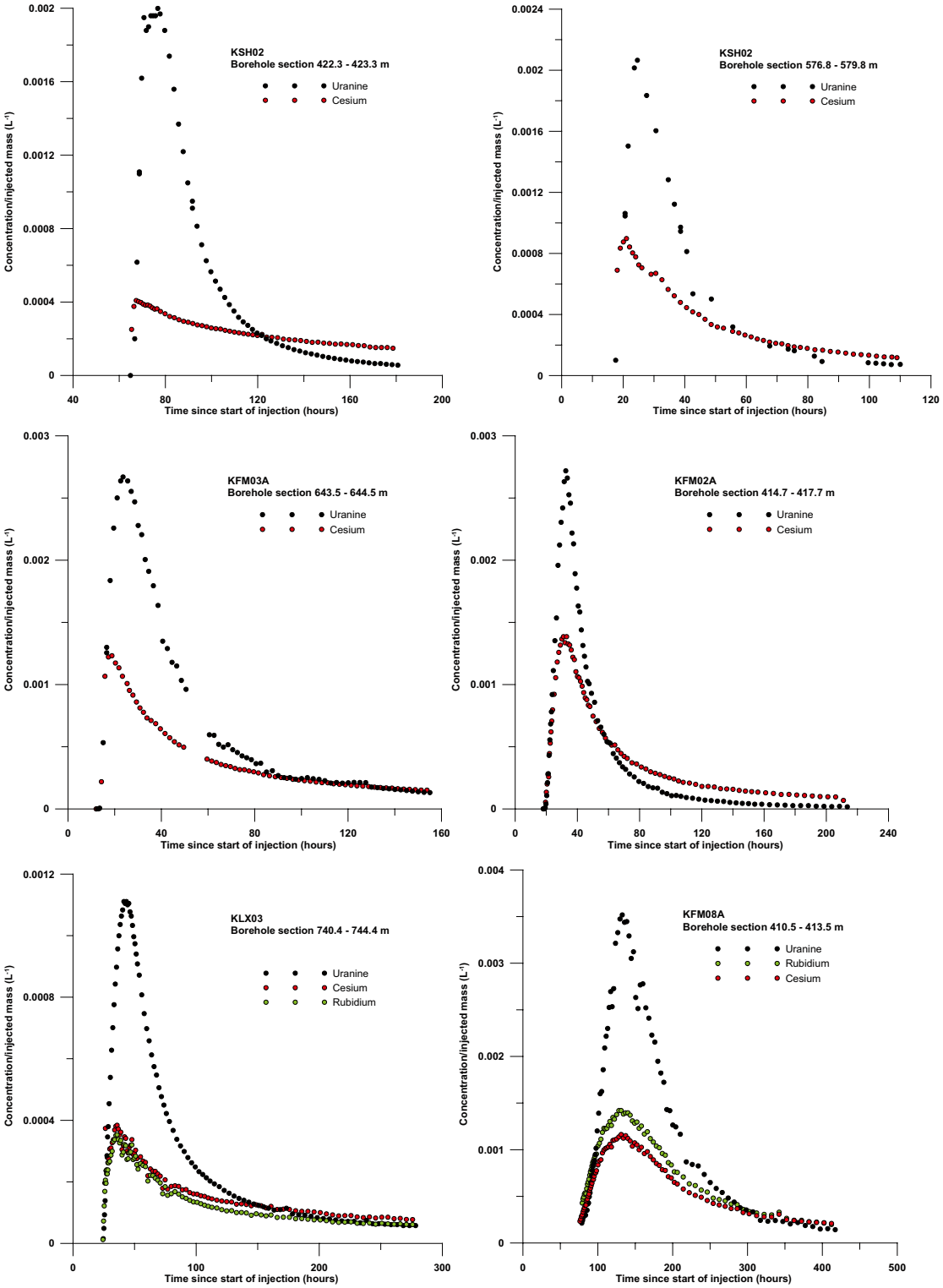

Figure 3-2. *Experimental results from the SWIW tests performed within the site investigation programmes.*

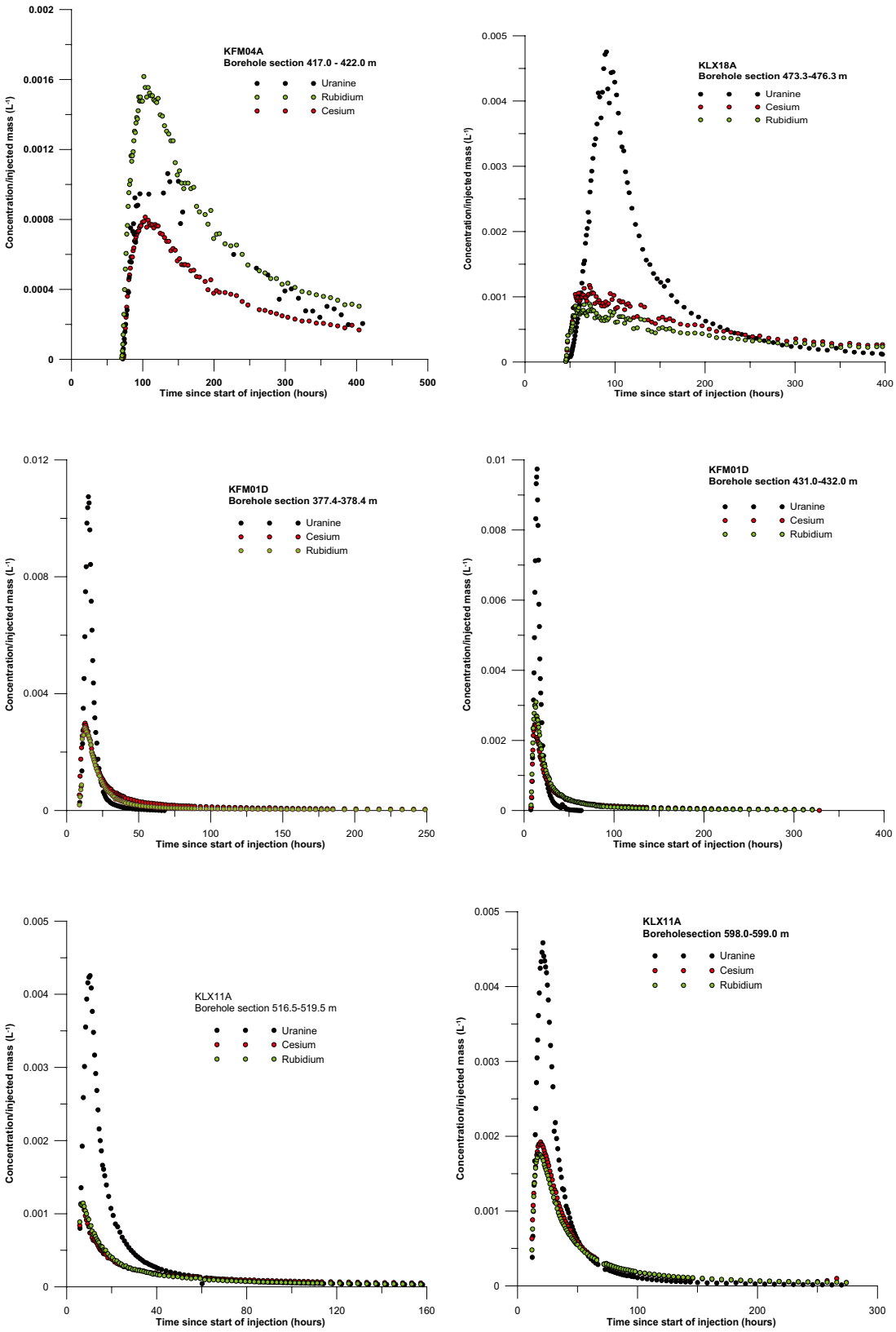

Figure 3-2. *(continued from previous page). Experimental results from the SWIW tests performed within the site investigation programmes.*

The experimental breakthrough data are judged to be of high quality. The breakthrough curves are fairly smooth and with very little experimental noise or other disturbances. Further, an immediate visual impression is that a very clear retardation effect of the sorbing tracers is indicated.

The tracer recovery is an interesting result because it is another indication of the quality of the experimental performance and test design. It is also very valuable for subsequent evaluation/modelling to have an indication of how much of the injected tracers are recovered during the recovery phase. The tracer recoveries at the end of the pumping phase for each test and tracer are presented in Table 3-4.

The estimates of tracer recovery from experimental data are in many of the tests limited by the fact that the recovery breakthrough curves are truncated due to the time frames allocated for each test. Thus, most of the estimates of tracer recovery are lower than the "true" recovery that would have resulted if pumping had continued until background values were reached. In a few cases (the tested section in KFM01D and KLX11A), the Uranine concentrations reach close to background values during the recovery pumping and in those cases the estimated recovery is close to or at 100 percent. In most other cases, the "true" tracer recovery is difficult to estimate, especially for the sorbing tracers, because there often is considerable tailing in the breakthrough curves. However, plausible extrapolations of the experimental breakthrough curves do generally not indicate that tracer recovery would not be complete. This is somewhat supported by the plot in Figure 3-3 where Uranine recovery is plotted against total pumped water volume during the recovery phase (given in units related to the total injected water volume). Figure 3-3 shows a fairly clear relationship between the Uranine recovery and the duration of the recovery pumping. The graph indicates that for 100% recovery, at least about 25 injection volumes would be required to be pumped back. The fairly well defined relationship indicated by Figure 3-3 also indicates that the tests with less than full recovery may have reached 100% with a longer pumping duration. The two sections in KFM01D deviates clearly from the indicated relationship and shows full recovery much earlier than what would be expected from most of the other tests. The two sections in KFM01D are in Figure 3-3 plotted as having reached 100% recovery at ten injection volumes, which should be regarded as a very approximate estimate. Another anomalous point is for the test in KFM04A (with 43% recovery). The Uranine recovery in KFM04A

Table 3-4. Tracer recovery at the end of the recovery pumping phase.

Borehole	Section (m)	Uranine (%)	Cesium (%)	Rb (%)
KSH02	422.3–423.3	86.2	40.7	–
KSH02	576.8–579.8	80.5	51.6	–
KLX03	740.4–744.4	89.9	51.8	43.6
KLX18A	473.3–476.3	86.8	46.4	36.7
KLX11A	516.5–519.5	98	45	43
KLX11A	598.0–599.0	95	72	68
KFM02A	414.7–417.7	86.9	83.3	–
KFM03A	643.5–644.5	78.6	44.3	–
KFM08A	410.5–413.5	81.1	50.1	42.4
KFM04A	417.0–422.0	42.6	53.9	32.8
KFM01D	377.4–378.4	104	92	68
KFM01D	431.0–432.0	102	87	90

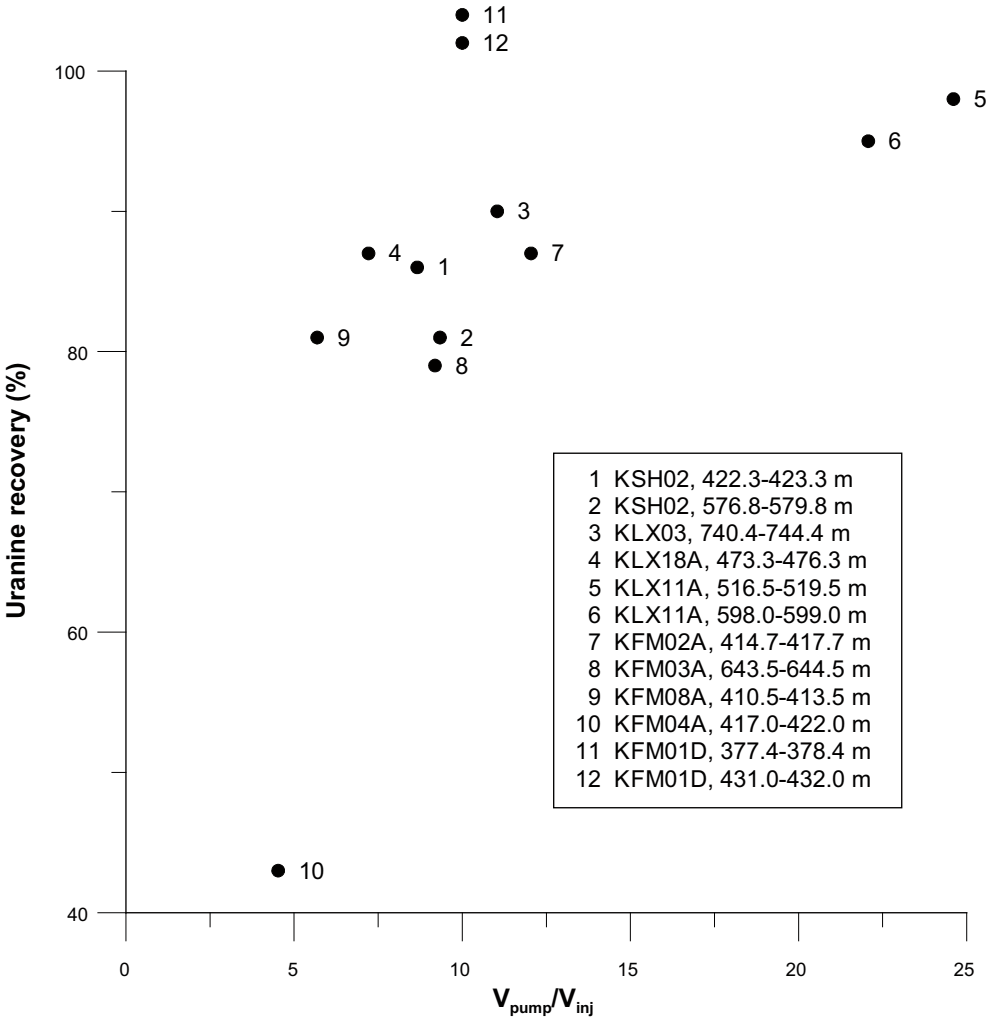

Figure 3-3. *Uranine recovery plotted versus total pumped water volume (V_{pump}) divided by total injected water volume (V_{inj}). The anomalous point (with 43% recovery) represents KFM04A. Note that both of the sections in KFM01D reach full recovery well before the end of the recovery phase, roughly estimated to about 10 injection volumes.*

was indeed concluded to be incomplete /Gustafsson et al. 2006c/. The most probable reason for the incomplete recovery in KFM04A is that Uranine has travelled through a connected network back into the borehole outside the packed-off test section. Note that for the sorbing tracers the tracer recovery may still indicate full recovery because those tracers have travelled shorter distances.

The corresponding plot for cesium is presented in Figure 3-4, which shows a similar relationship as in Figure 3-3 except that there is more scatter in the plotted recovery values. The increased scatter reflects the varying sorption effect of cesium (as shown in section 3.3), i.e. the recovery for a given pumping volume depends on how strongly Cs is sorbed.

In subsequent evaluation (modelling) of the SWIW tests, it has generally been assumed that full recovery of all non-sorbing as well as sorbing tracers had been obtained if the recovery pumping had been continued until background levels were reached.

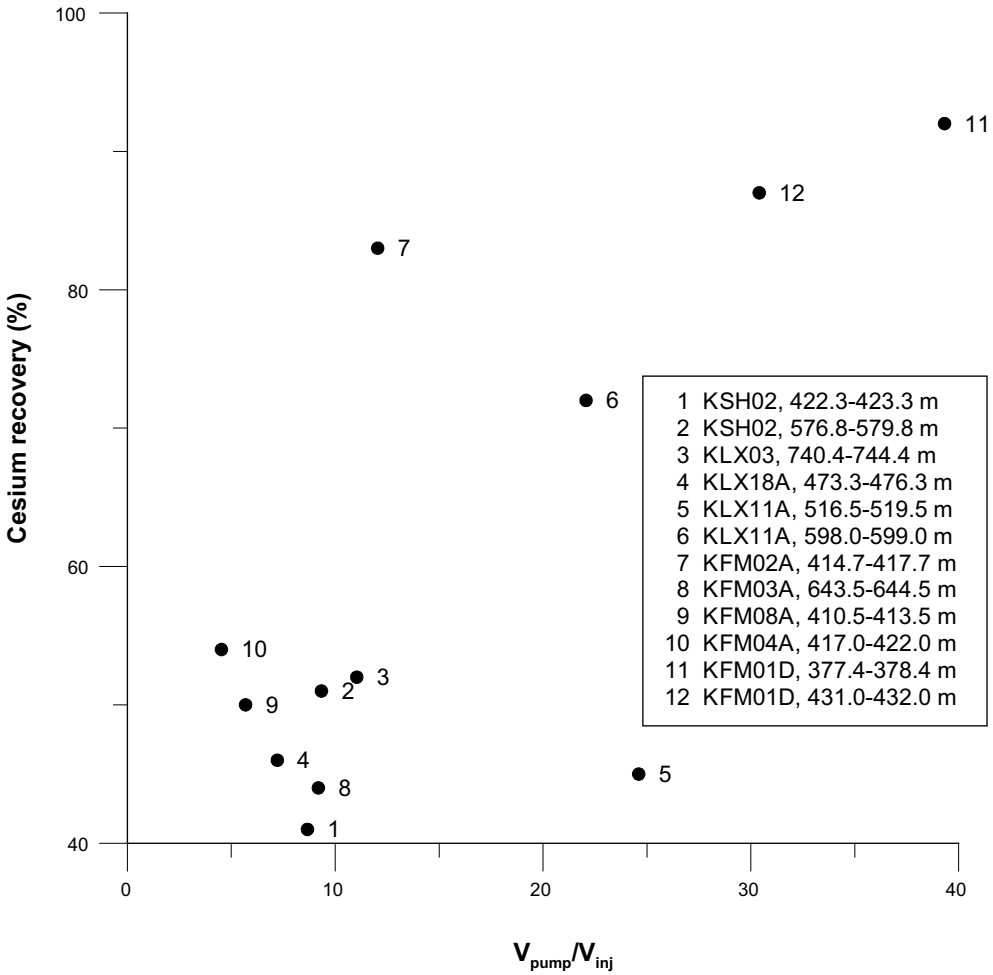

Figure 3-4. *Cesium recovery plotted versus total pumped water volume (V_{pump}) divided by total injected water volume (V_{inj}).*

A more detailed illustration of the Uranine recovery is shown in Figure 3-5, where the experimental breakthrough curves are plotted as fractional recovery against pumped volume/total injected volume. Figure 3-5 facilitates a comparison of the transient recovery of the various tests. The plot shows both of the tested sections in borehole KFM01D attain full recovery after relatively few pumped back injection volumes, and these sections are also significantly different than the other sections. Further, there are three sections (KFM03A, KSH02 576.8–579.8 m, KLX03), disregarding KFM04A, that appears to have a somewhat slower recovery. For the rest of the tests, the transient recovery behaviour is fairly similar, except for KFM02A, which appears to flatten out around 80%.

It may be argued from a visual inspection of the recovery curves in Figure 3-5 that one can not exclude full recovery in any of the tests (disregarding KFM04A), except possibly in KFM02A for which the recovery curves appear to level out somewhat at values between 80 and 100% recovery.

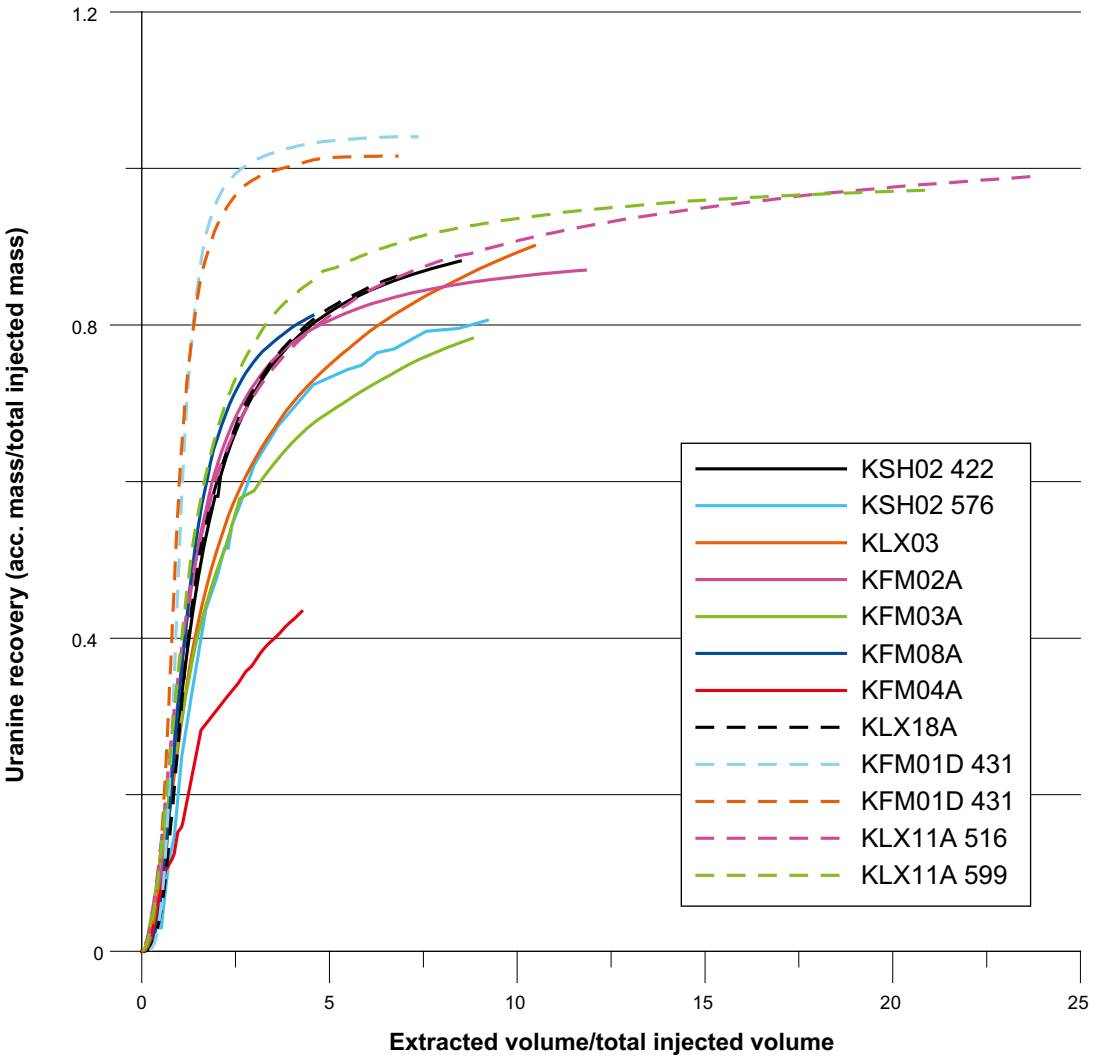

Figure 3-5. *Fractional tracer recovery of Uranine for all of the SWIW tests performed within the site investigations.*

The corresponding recovery breakthrough curves to Figure 3-5 are shown in Figure 3-6, where each breakthrough curve is normalised so that the area of each curve is equal to one at full recovery. Figure 3-6 provides further comparison of the various SWIW tests. As indicated above, the results from both of the SWIW tests in KFM01D are significantly different than from the other tests, with steeper curves and significantly higher peaks. Further, KFM04A also deviates because of incomplete tracer recovery, as discussed above. The peaks for all of the curves appear at approximately one recovered injection volume.

A brief summary of the experimental data from the SWIW tests is that data appear to be of high quality with smooth breakthrough curves without excessive noise or other irregularities. The tracer recovery has generally been found to be high; for the tests with less than full recovery at the end of pumping, it is generally indicated that full recovery would have been obtained if pumping had continued. The only obvious exception is Uranine recovery in KFM04A, where it is concluded that a significant amount of Uranine is lost during the experiment.

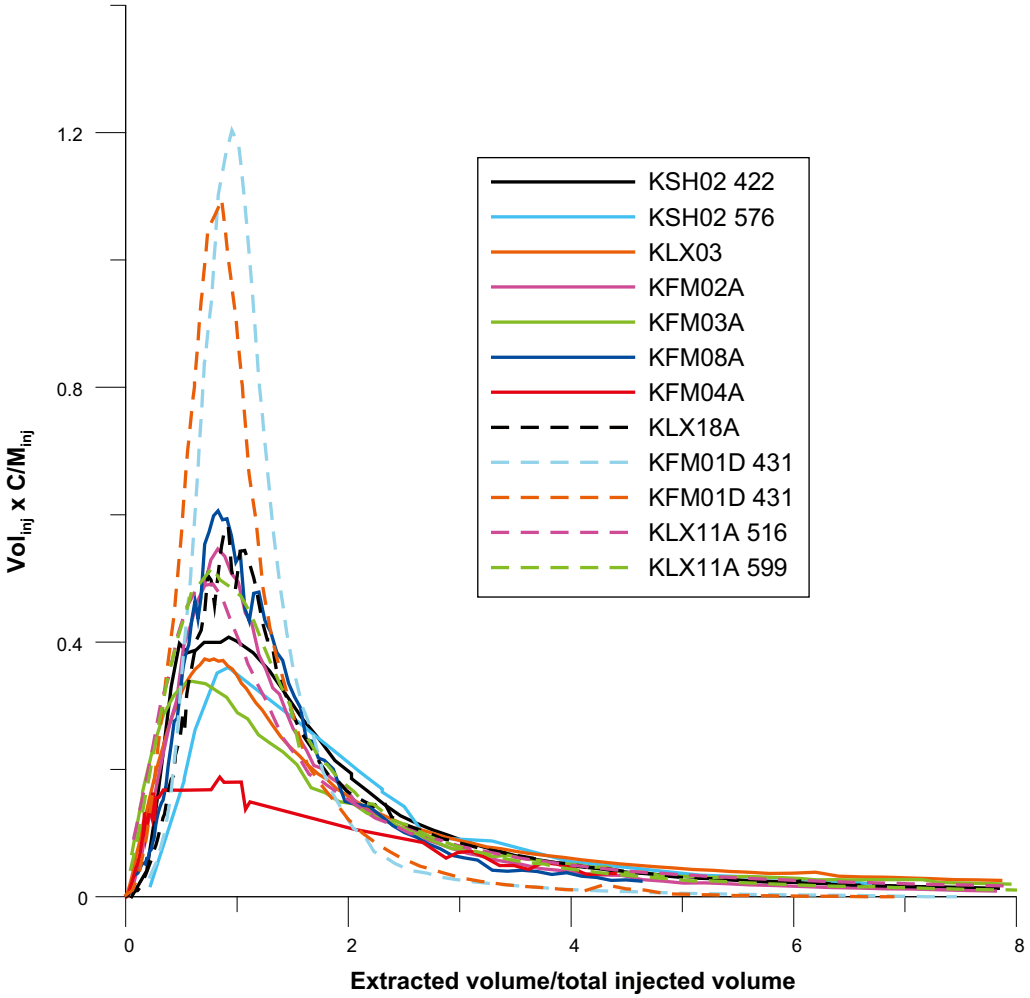

Figure 3-6. *Comparison of Uranine breakthrough data from all SWIW tests performed within the site investigations. The plot variables are scaled so that the area of each curve is equal to one at 100% tracer mass recovery.*

3.4 Previous basic evaluation of the SWIW tests

All of the SWIW tests within the site investigation programmes have been subject to a basic model evaluation. Model assumptions comprised 1-dimensional homogenous radial flow and transport in a single fracture (or fracture zone) with advection, dispersion and linear equilibrium sorption as the only processes affecting tracer transport. No effects of diffusion into stagnant water or sorption in a porous matrix were considered in this evaluation. The numerical simulation model SUTRA /Voss 1984/ was employed, where model input describing the experimental phases was specified as carefully as possible using documentation from the experimental field work. Generally, experimental flows and durations may vary from one phase to another, and the flow may also vary within phases.

Model simulation results were fitted to experimental field data using weighted non-linear regression. The non-sorbing tracer (Uranine) was fitted simultaneously with a sorbing tracer (cesium and/or rubidium). Estimation parameters comprised longitudinal dispersivity (for fixed values of fracture aperture/porosity) and a fracture retardation factor for the sorbing tracer.

Examples of fits between model and experimental data for the various SWIW tests are shown in Figure 3-7 (Uranine and cesium) and in Figure 3-8 (Uranine and rubidium). Due to incomplete Uranine mass recovery /Gustafsson et al. 2006c/, no evaluated parameter values were reported for borehole KFM04A.

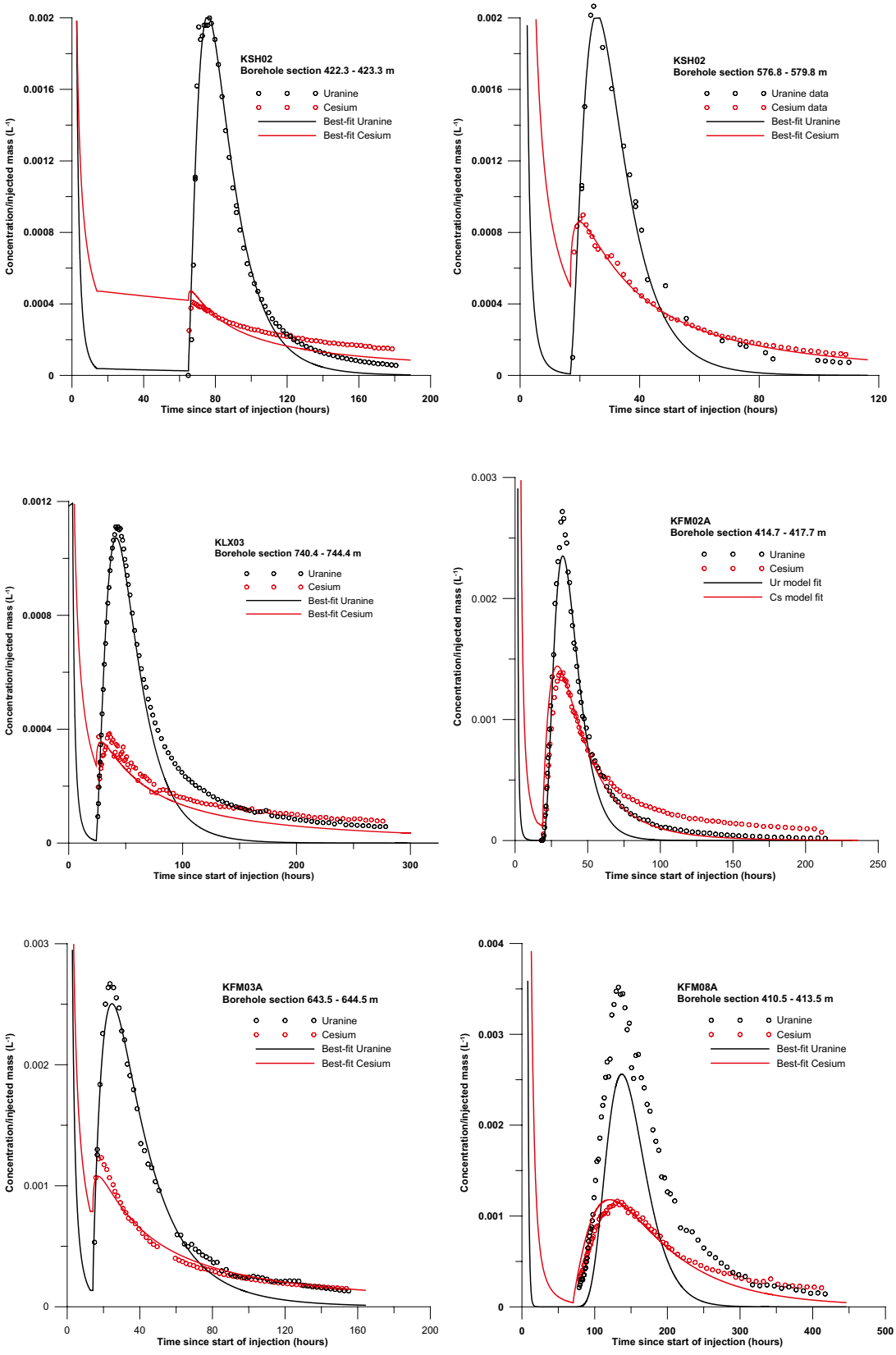

Figure 3-7. *Model evaluation of Uranine and cesium for SWIW tests within the site investigation programmes (no model evaluation of cesium was made for KFM04A).*

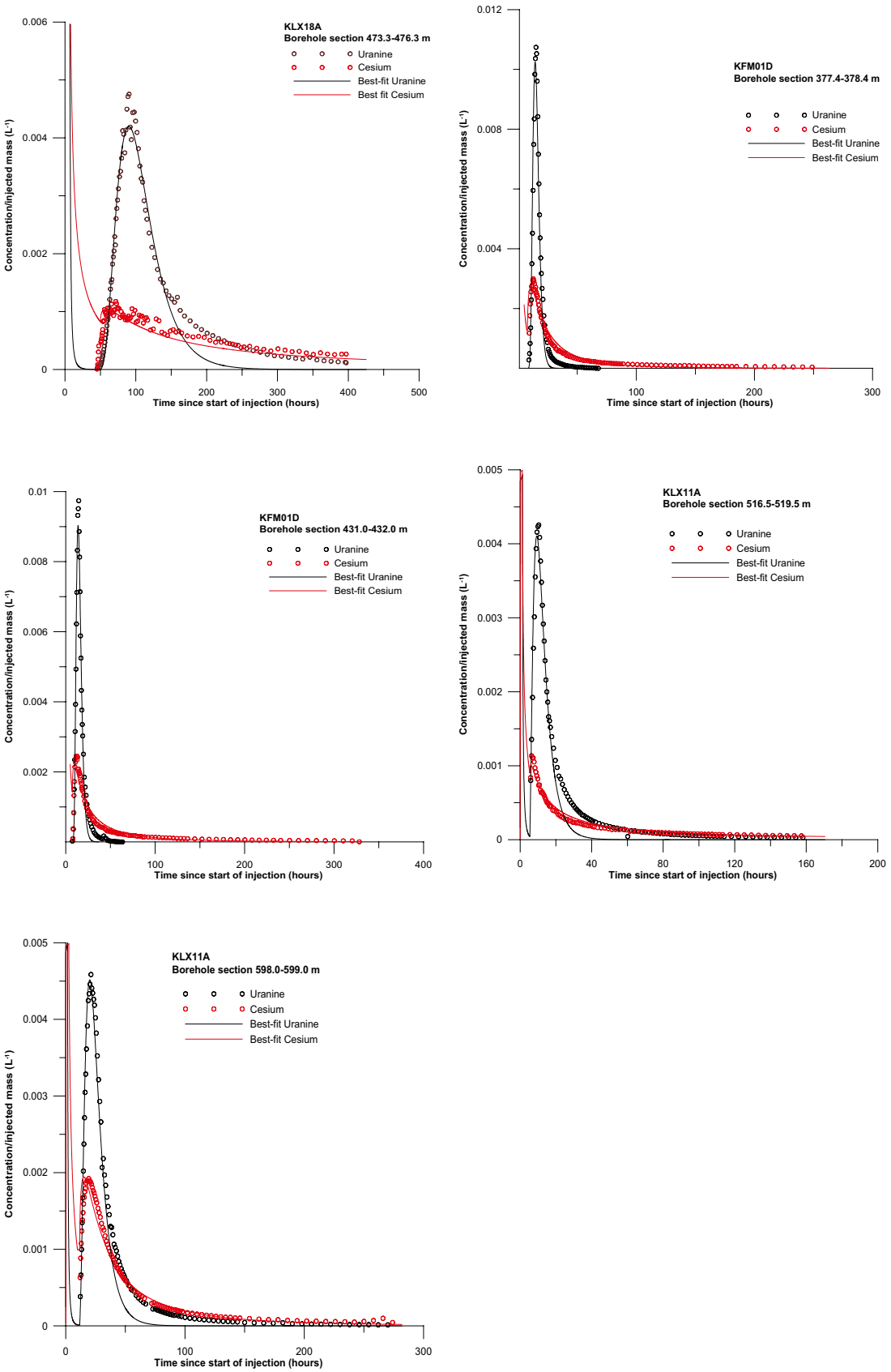

Figure 3-7. *(continued from previous page). Model evaluation of Uranine and cesium for SWIW tests within the site investigation programmes (no model evaluation of cesium was made for KFM04A).*

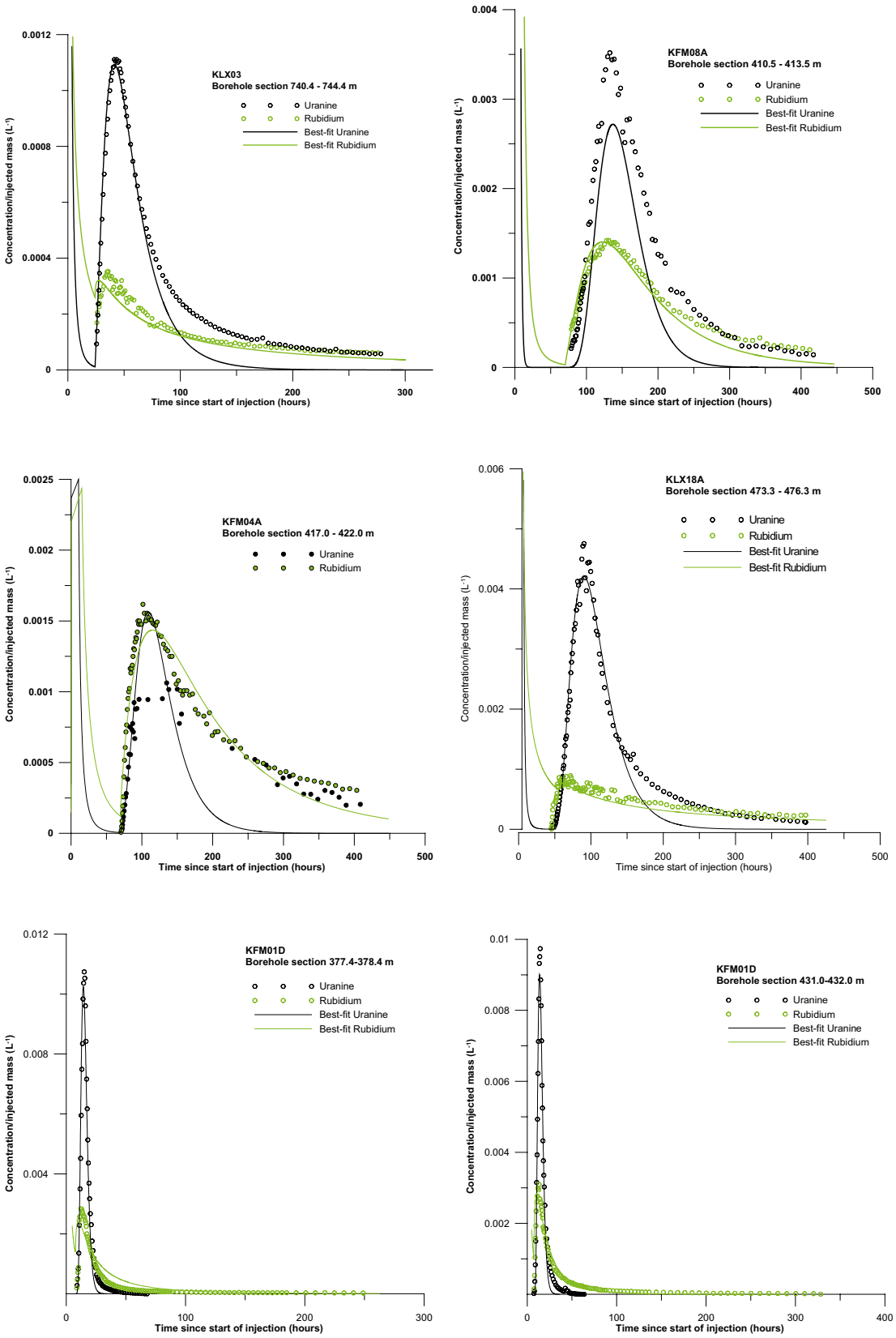

Figure 3-8. *Model evaluation of Uranine and rubidium for SWIW tests within the site investigation programmes (no model evaluation of rubidium was made for KFM04A).*

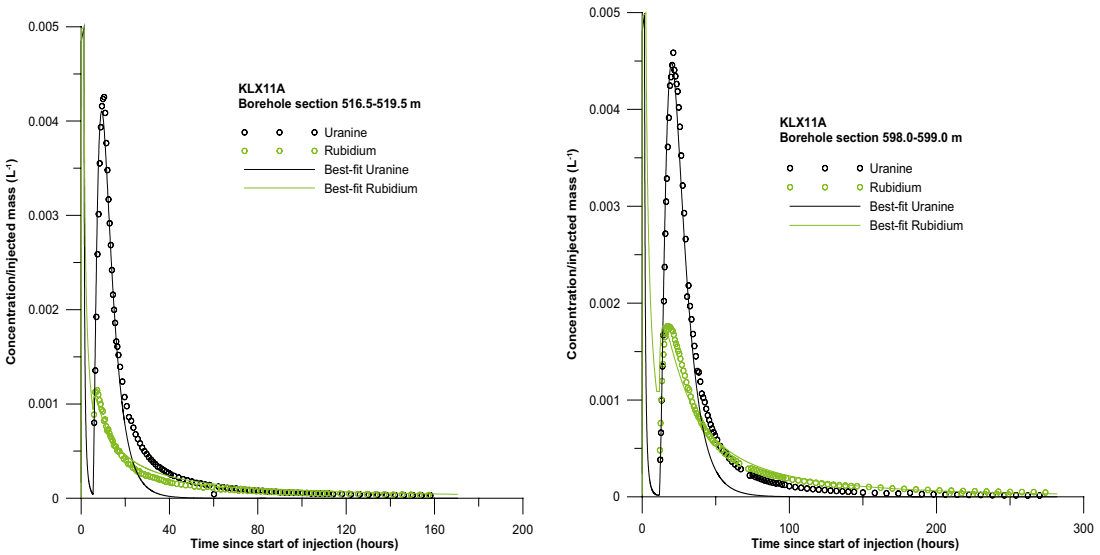

Figure 3-8. *(continued from previous page). Model evaluation of Uranine and rubidium for SWIW tests within the site investigation programmes (no model evaluation of rubidium was made for KFM04A).*

A brief visual inspection of the fits in Figures 3-7 and 3-8 gives the overall impression that it is possible to obtain a relatively good fit to experimental data with the simple advection-dispersion model. The non-sorbing and sorbing tracers are fitted simultaneously, where the only difference between simulated curves is that the sorbing tracer is assigned a simple retardation factor (linear equilibrium sorption). The only major discrepancy between model and data is that there appears to be a consistent lack of fit in the tailing parts of the Uranine curves.

The results from the basic model evaluation are summarised in Table 3-5. Before discussing the results further, however, some remarks about the relationship between dispersivity and porosity/aperture from SWIW tests should be made.

Porosity/aperture and dispersivity may not both be independently estimated from a SWIW experiment, unlike in a cross-hole tracer experiment. One may view this as lacking a transport length reference, i.e. it is not known how far into the formation the tracer has travelled during a SWIW experiment (unless other observation boreholes are available for this purpose).

The exact relationship between these two parameters is, generally, dependent on the experimental configuration and in which way observations are made. For example, given a specific governing equation, the identifiability of parameters is different in a cross-hole test compared with a SWIW test. In a cross-hole test, dispersivity and porosity/aperture/velocity may be obtained when evaluating the breakthrough curve while only one of the parameters may be obtained from a SWIW experiment.

The analytical solution for a SWIW test derived by /Gelhar and Collins 1971/ may be used to indicate that the dispersivity and porosity are components in a lumped parameter in which the total injected water volume also appears. The lumped dimensionless dispersion parameter, herein called τ, may be written as:

$$\tau = \frac{a_L^2 \delta}{V_{inj}} \qquad (3\text{-}2)$$

where a_L is the longitudinal dispersivity [L], δ is the equivalent fracture aperture [L] and V_{inj} is the total injected water volume (injection + chaser phases) [L^3]. The aperture may alternatively be expressed using the product of porosity and thickness. In a homogenous radial flow system with advection and dispersion as the only transport processes, this lumped parameter determines the shape of a SWIW breakthrough curve.

Table 3-5. Summary of results from the basic evaluation. Evaluation parameters are given as dimensionless dispersivity (τ, equation 3-2) and retardation factors (R) for cesium and rubidium, respectively.

Borehole	Section (m)	$a_L^2\ \delta/V_{inj} \times 10^{-3}$	R	
			Cesium	Rubidium
KSH02	422.3–423.3	5.7	975	–
KSH02	576.9–579.8	3.8	87	–
KLX03	740.4–744.4	3.9	235	390
KLX18A	473.3–476.3	1.2	857	2,700
KLX11A	516.5–519.5	3.8	808	622
KLX11A	598.0–599.0	2.8	66	105
KFM02A	414.7–417.7	1.3	11	–
KFM03A	643.5–644.5	12	73	–
KFM08A*	410.5–413.5	0.23	34	20
KFM04A**	417.0–422.0	–	–	–
KFM01D	377.4–378.4	0.17	535	930
KFM01D	431.0–432.0	0.29	918	238

* The KFM08A SWIW test resulted in poor model fits and results should be considered uncertain /Gustafsson et al. 2006b/, compared with the other sections.

** The KFM04A SWIW test resulted in a substantial loss of Uranine during the experiment and no evaluated parameter values were reported /Gustafsson et al. 2006c/.

Table 3-5 shows a large variation in evaluated retardation factors for cesium and rubidium. The smallest value of R is found in KFM02A (R = 11) and the largest in KSH02, 422.3–423.3 m (R = 975). For rubidium, there is a very large value in KLX03 (R = 2700) while the lowest value is found in KFM08A (R = 20) although the retardation factors for KFM08A are considered more uncertain than the rest of the R values in Table 3-5 /see Gustafsson et al. 2006b/. There is no obvious pattern of the relative retardation strength between the two sorbing tracers.

The evaluated dispersion parameter, τ, ranges in most cases from 1 to 5. Exceptionally low values (i.e. low dispersion effect) are found in both of the sections in KFM01D and a high value (12) is obtained for the section in borehole KFM03A. The low value in KFM08A should be considered uncertain /see Gustafsson et al. 2006b/. In order to illustrate the dimensionless dispersivity further, the results are plotted as longitudinal dispersivity vs. aperture for each of the evaluated SWIW tests in Figure 3-9. Figure 3-9 shows that for an aperture value of 0.001 m, the longitudinal dispersivity for the tested section in KFM02A, for example, would be about 0.5 m.

It should be noted that the relationship discussed here between porosity/aperture and dispersivity is particular to the applied model, where the dispersion is simulated as a velocity-dependent process. This relationship may be different for other conceptual models of dispersion.

A brief summary of the basic evaluation using a simple one-dimensional advection-dispersion model with linear equilibrium sorption, where the non-sorbing tracer and a sorbing tracer are fitted simultaneously, shows that a relatively good fit of model to experimental data is obtained for most of the experimental data. However, there is a systematic lack of fit in the tailing parts of the non-sorbing tracer (Uranine), apparently irrespective of experimental conditions (experimental flows, durations, etc). For the sorbing tracers, on the other hand, model fit to experimental data appear in many cases to be relatively good for the entire breakthrough curve.

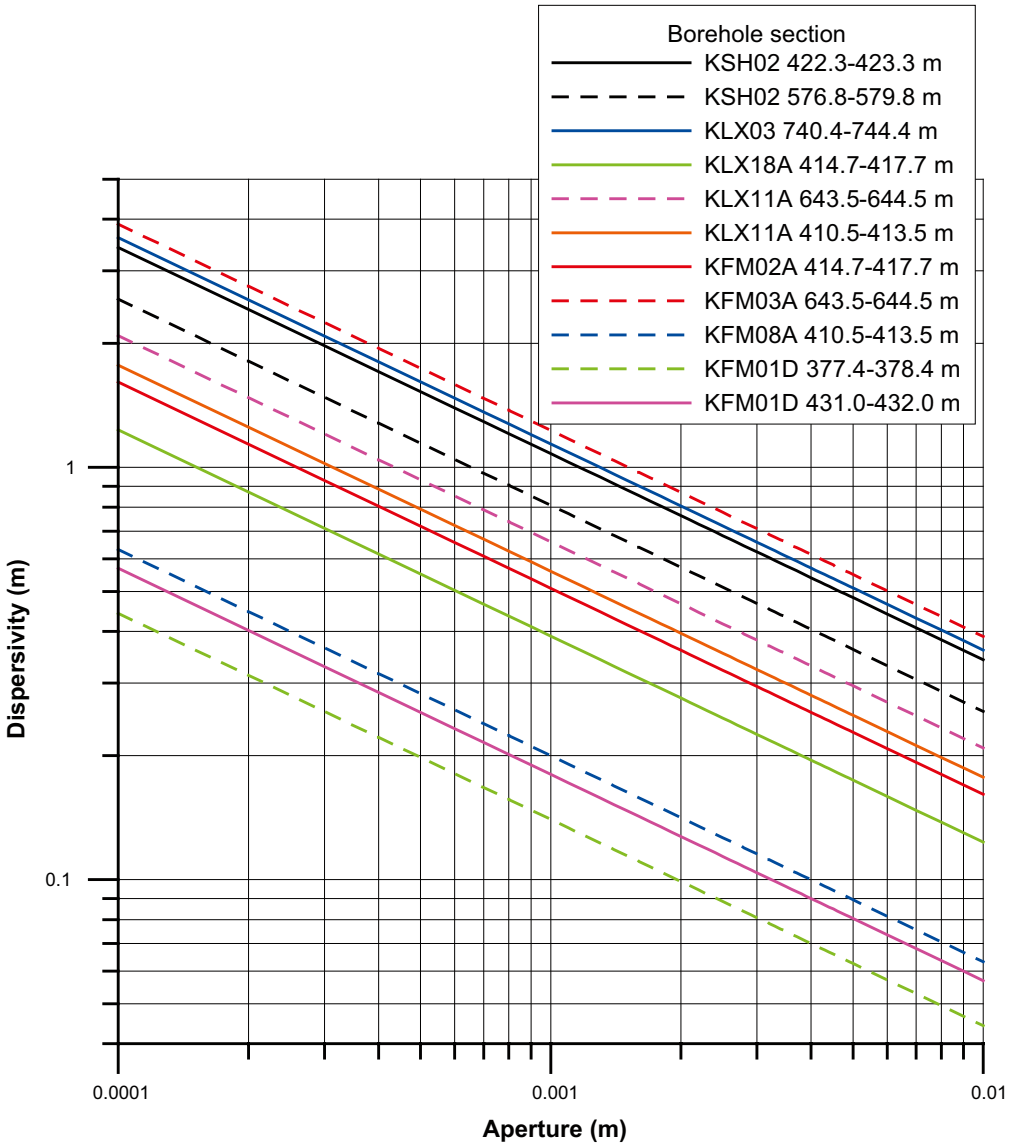

Figure 3-9. *Illustration of the relationship between longitudinal dispersivity and aperture (equation 3-2) for all of the evaluated SWIW tests within the site investigation programs.*

It is possible to hypothesize several reasons why Uranine consistently shows a lack of fit in the tail of the recovery breakthrough curve. There may be effects of experimental equipment and procedures, such as, for example, solute storage in stagnant equipment volumes and tubing dispersion. Other reasons are more conceptual, i.e. there may be geometrical features and/or properties of the rock/fracture domain as well as transport processes that the applied simple model does not account for. In the next chapter, various potential effects of experimental procedures and equipment are discussed. Following this in chapter 5, an extended evaluation with a simple model including matrix diffusion and matrix sorption is presented.

4 Possible effects of equipment and experimental procedures

4.1 Overview of possible effects/artefacts

In this section, some potential effects of experimental procedure and/or equipment on experimental results are discussed. These include:

- Mixing in the borehole section. Mixing conditions in the tested borehole section differ between injection and sampling.
- Tubing dispersion. The length of the tubing used for tracer injection and sampling is considerable, about 300–700 m.
- Natural flow through the borehole. Although this is not an experimental "artefact", one should be aware of that a large background flow may influence the results.
- Other storage effects in stagnant parts of borehole section or experimental equipment.

The listed factors are discussed in more detail below.

4.2 Mixing and dispersion in borehole section and tubing

Below follows a brief description of how the experimental equipment and procedures may influence the tracer content during the various phases. For the SWIW tests performed within the site investigation programmes, the following main features of tracer injection and sampling are:

1. Establishment of steady injection flow conditions prior to injection of tracer. This only provides controlled hydraulic conditions and does not affect the other parts of the SWIW experiment.
2. Tracer injection: tracer is injected at the ground surface; travels through the borehole tubing and enters the borehole section. The borehole section is equipped with dummies (to minimise volume) and is continuously stirred using a re-circulation system. The borehole volume (restricted by the dummies in the section) and the volume in the tubing and equipment for re-circulation comprise the total mixing volume for the tracer in the borehole section. Tracer residence times in the tubing from the ground surface to the borehole section are often longer than the injection duration. Thus, at the end of the tracer injection at the ground surface, most of or all of the tracer is actually still in the borehole tubing between the ground surface and the test section. The tracer then enters the borehole section during the first part of the chaser injection period. The travel times in the tubing need be accounted for when evaluating the experimental results. In addition, the continuously stirred borehole section also modifies the tracer input (to the tested rock formation) in such a way that the theoretical input pulse is transformed to a typical CSTR (continuously stirred tank reactor) output.
3. Chaser fluid injection: tracer-free water is added to the borehole section in the same manner as in the preceding step. Because the borehole section still is continuously stirred by the re-circulation system, the remaining tracer in the borehole will be added to the tested rock formation as a decaying pulse.
4. Waiting phase (when employed): No water is added to the section and no circulation is made of the water in the borehole section.

5. Recovery/sampling phase: The water in the borehole section is not re-circulated and mixing in the section is therefore limited. The pumped water flows, presumable as a plug flow, from the tested fracture(s) to the top of the section, where the pumping inlet is located. The pumping inlet is located immediately above the dummy placed inside the tested section and is connected to a device that distributes the pumped water evenly along the perimeter of the dummy. Depending on the distance from the sampling point to the flowing fracture(s) in the section, there will be some volume of borehole section water that enters the tubing before water from the tested rock formation enters the tubing. However, this volume is relatively small compared with the total volume injected. Further, one should consider the residence time in the tubing from the pumped section to the ground surface, where the sampling is made. Tubing residence times for the recovery phase, as well as the injection phases, typically ranges from about one hour to a few hours.

Another mechanism that one needs to consider is dispersion in the tubing. Under laminar flow conditions in the tubing, effects of dispersion during the water transport through the tubing may be considerable. In short-term tracer tests, i.e. where the tracer residence times in the rock formation is not significantly larger than the tubing residence times, this effect may need to be accounted for.

4.2.1 Mixing in the borehole section

Mixing conditions for tracers in borehole sections used for injection and pumping are important to consider in all types of tracer experiment, cross-hole tests as well as single-hole tests. There exists a variety of methods for tracer injection and sampling that may be employed to ensure a successful performance of the tracer test.

During the first two steps in a SWIW test, tracer injection and chaser injection, a rectangular tracer pulse added to the borehole section will be altered before entering the fracture(s) intended to be investigated by the SWIW test. Assuming a well stirred borehole section, the effect on the tracer input pulse may be estimated by a simple mixed-tank calculation:

$$C(t) = (C_0 - C_{in}) \exp\left[\frac{-Qt}{V_{bh} + K_a A_{bh}}\right] + C_{in} \qquad 0 \le t < t_{inj} \qquad \text{(4-1a)}$$

$$C(t) = C(t_{inj}) \exp\left[\frac{-Q(t - t_{inj})}{V_{bh} + K_a A_{bh}}\right] \qquad t_{inj} \le t < t_{chase} \qquad \text{(4-1b)}$$

where C(t) is concentration in water leaving the borehole section and entering the formation [M/L^3], V_{bh} is the borehole volume including circulation tubing [L^3], A_{bh} is area of borehole walls [L^2], Q is flow rate [L^3/T], C_{in} is concentration in the water entering the borehole section [M/L^3], C_0 is initial concentration in the borehole section [M/L^3], K_a is a surface sorption coefficient [L], t is elapsed time [T], t_{inj} is the time at the end of the injection phase [T] and t_{chase} is the time at the end of the chaser phase [T].

The borehole mixing effects during tracer injection and chaser phases are illustrated in Figure 4-1. The tracer injection duration in Figure 4-1 is set to 50 minutes which is fairly typical for the SWIW tests carried out within the site investigations.

In all model simulations shown in section 3.2 as well as in chapter 6, this mixing process is accounted for in the simulations. If the total experimental time frame of each performed SWIW test is long compared with the injection duration, the effect of mixing in the borehole section on the recovery breakthrough curve is relatively small. However, for some of the SWIW tests with relatively short tracer injection and chaser injection durations, this effect may be significant enough to be accounted for in the simulations.

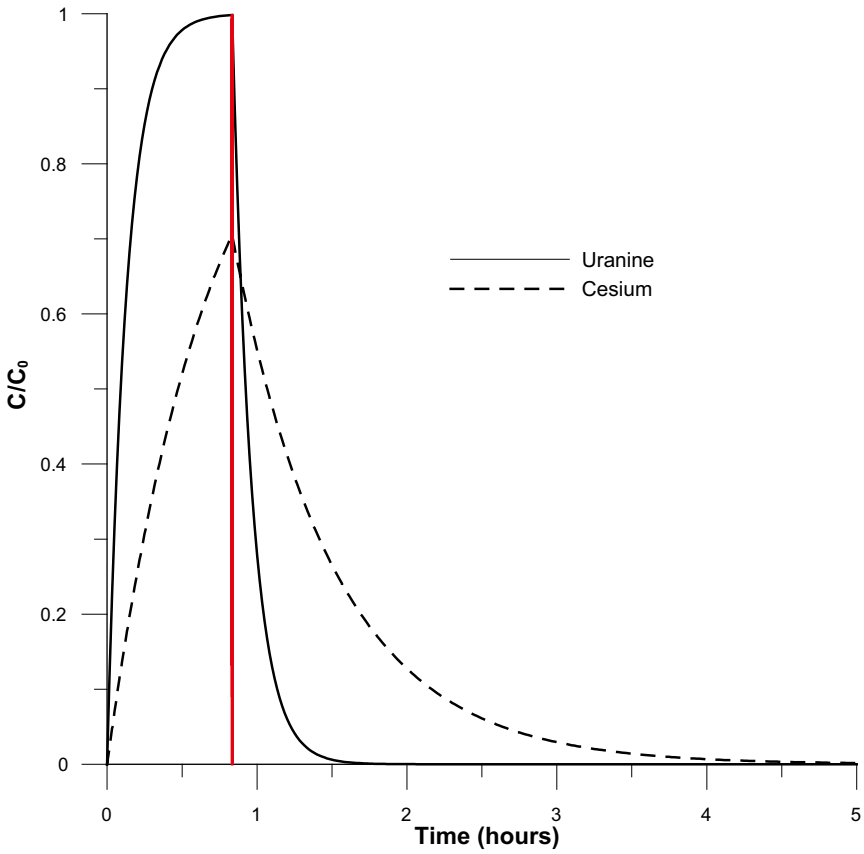

Figure 4-1. *Example of simulated tracer injection functions for a tracer injection phase (ending at 50 minutes shown by the vertical red line) immediately followed by a chaser phase.*

During tracer recovery phase, when the tracer is pumped back to and into the borehole section, there is no circulation of the water in the borehole section. The inlet of the sampling tube is placed at the top of the section. The inflowing water from the fracture(s) flows with minimal mixing along the volume separated by the borehole dummy and the borehole wall to the inlet of the sampling tube. This means that at the very beginning of the recovery pumping, the pumped water is not representative for what comes out of the tested fracture formation. Instead, one should expect that some of the early samples are diluted (because the borehole section should be free of tracer after the chaser injection phase) to various extent, depending on where the inlet is placed in relation to the flowing features. For most of the performed SWIW tests, a very rough estimate is that samples may be affected by such dilution effects during the first 10–30 minutes. For a few sections with low recovery pumping flow and relatively long test sections, this effect may extend up to the first 1–2 hours of sampling.

The SWIW experiments in this report were made in core boreholes with a typical diameter of about 0.076–0.077 m. The borehole dummy placed inside the experimental section, in order to reduce the experimental volume, has a diameter of 0.073 m. For the borehole diameter range above, this results in section volumes of about $3.5–4.7\times10^{-4}$ m^3/m section. In addition to this, water in hoses, filters and the dilution probe adds about 0.0008–0.001 m^3 to the total experimental volume. The total experimental section volumes among all of the SWIW tests roughly varies within the range of 0.001–0.003 m^3. The correspondning borehole wall area is then about 0.24 m^2/m section.

4.2.2 Dispersion in tubing

The experimental set-up for SWIW tests within the site investigation programmes entails tracer injection and water sampling at the ground surface via tubing down to the tested borehole section. Because of the considerable tubing distance involved, it is justified to ask whether dispersion effects in the tubing might affect the interpretation of the tests. The evaluation of the tests has so far been carried out with the assumption of ideal plug flow in the tubing, and experimental data have been corrected for tubing residence times but not for dispersion in the tubing.

In order for dispersion to have a significant effect on tracer transport in the tubing, laminar flow conditions are required. The boundary between laminar and turbulence flow is given by the Reynolds number (Re). The Reynolds number for a cylindrical flow channel is:

$$\mathrm{Re} = \frac{v d_{tube}}{\upsilon} \tag{4-2}$$

where v is the average velocity [L/T], d_{tube} is the tube diameter [L] and υ is the kinematic viscosity [L^2/T]. The flow regime is laminar for Re < 2,000 and turbulent for Re > 2,000 /de Marsily 1986/.

For the SWIW tests reviewed in this report the Reynolds number in the tubing vary from about 90 to 670. Thus, it should be safe to assume that laminar flow conditions dominate during the various injection and pumping phases.

For laminar flow conditions, dispersion occurs in the tubing because the velocity at the centre of the tube is larger than the velocity along the tubing wall. The effective dispersion coefficient, $D_{tube,}$ for a cylindrical tube may then be given by /Bear 1988/:

$$D_{tube} = \frac{(d_{tube}/2)^2 v^2}{48 D_W} \tag{4-3}$$

where D_w is the molecular diffusion coefficient [L^2/T].

As an illustration of the effect of tubing dispersion, the SWIW-test in KLX11A, section 516.5–519.5 m is used. This test is selected for this example because it is one of the shorter tests, with relatively high injection and pumping flows, thus also having large tubing velocities. This test also has the highest ratio between injection duration and total injection (injection + chaser) time. The following values/assumptions are used in this case:

- tubing length = 619 m,
- tubing residence time = 0.94 hours,
- tubing diameter = 0.06 m,
- $D_w = 5\times10^{-10}$ m^2/s (Uranine), /Ohlson and Neretnieks 1995/.

This results in a value of D_{tube} of approximately 12.4 m^2/s, which corresponds to a Peclet number of about 9.

In the sample calculation below of tubing dispersion effects, a standard one-dimensional advection-dispersion transport model is used for the tubing transport parts, with the values given above of tubing residence time and Peclet number as input parameters.

Effects in injection section

Figure 4-2 illustrates the effect of tubing dispersion for the example with KLX11A, section 516.5–519.5 m. The transport through the tubing with dispersion has been calculated with a standard one-dimensional transport model with input values as given above and an injection duration of about 0.86 hours.

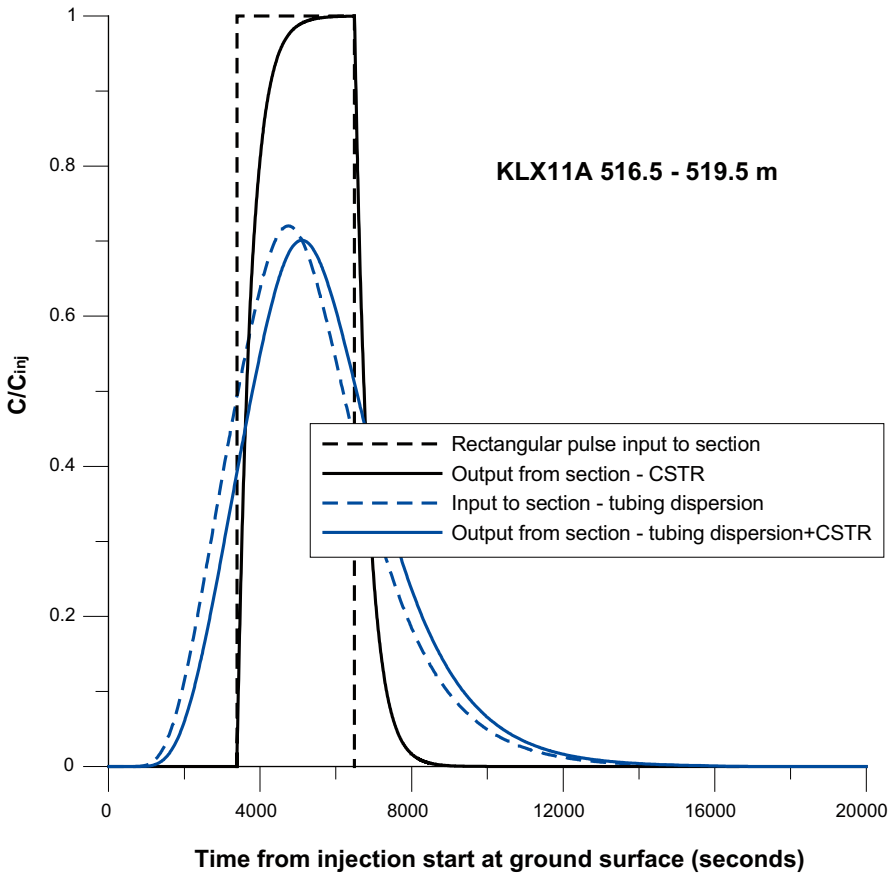

Figure 4-2. *Illustration of effect of tubing dispersion in injection section.*

Figure 4-2 shows a pure pulse input (dashed black line) and the corresponding case when the pulse input is modified by tubing dispersion is shown by the dashed blue line. Output from the section (i.e. into the fracture formation) is shown by solid lines, in both of the cases the output has been modified with CSTR (continuously stirred tank reactor) mixing (see section 4.2.1).

The effect of tubing dispersion is in this case that the input pulse is significantly modified and the dispersion effect on the output from the section is considerably more significant than from continuous mixing only.

Effect of injection function on the recovery breakthrough curve

The effect of tubing dispersion during tracer injection on the resulting breakthrough curve during recovery pumping is shown in Figure 4-3 and indicates that the effect is very small. This result indicates that the experimental time scale during the site investigation SWIW tests is too long, compared with tubing residence times, for tubing dispersion and/or mixing mechanisms in the borehole during tracer injection to have any significant effect on the tracer breakthrough in the borehole section during recovery pumping.

Effects on sampling during the recovery pumping

The last example shows the effect of tubing dispersion on sampling during the recovery phase (Figure 4-4). As the input breakthrough curve to the sample tubing, a simulated curve from this section is used and a 1-D advection-dispersion model is used to simulate the dispersion effect through the tubing to the sample collection at the ground surface. The effect of tubing dispersion on the sampling during recovery pumping is here very small because the time span of the breakthrough curve entering the tubing is large compared with the residence time in the tubing.

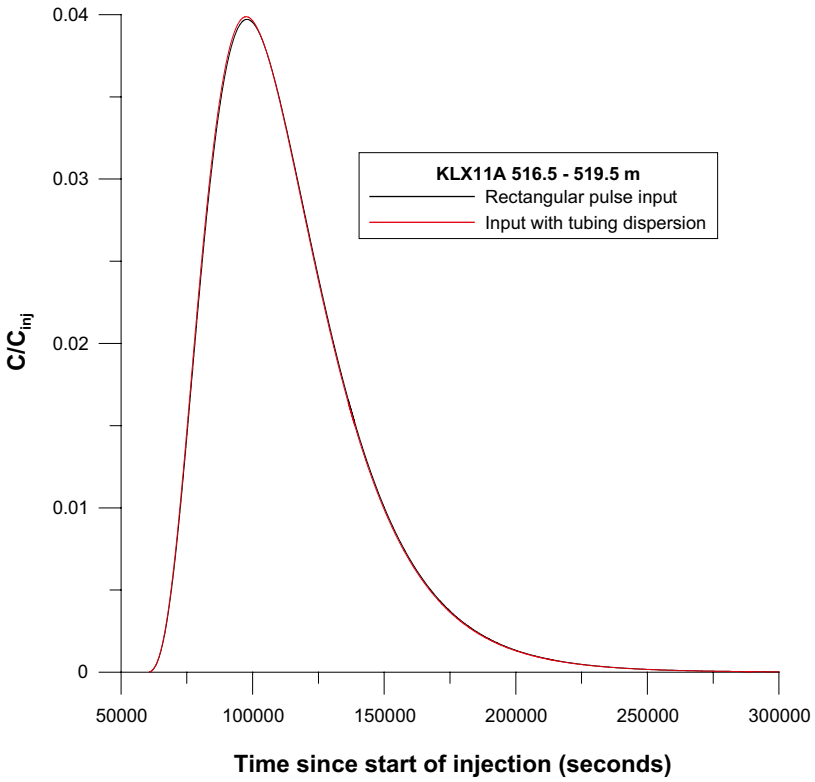

Figure 4-3. *Effect of tubing dispersion on the recovery breakthrough curve in the tested borehole section.*

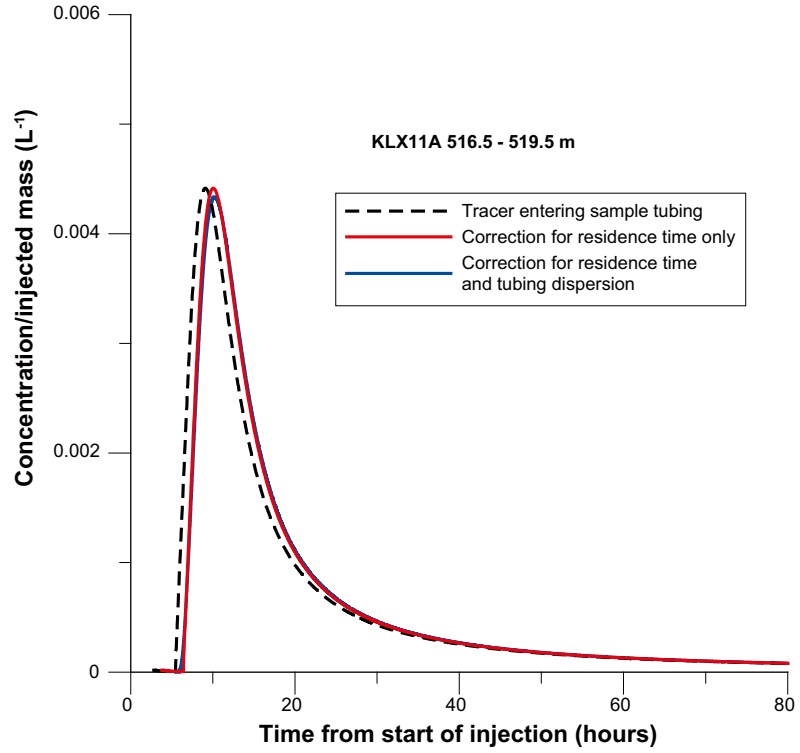

Figure 4-4. *Effect of tubing dispersion on sampling during recovery pumping.*

4.3 Solute storage in stagnant experimental volumes

There are some potential stagnant storage volumes that might cause "artificial" transient solute storage during a SWIW test. During the injection phase, the borehole section itself is continuously stirred and flushed out by the chaser fluid for a relatively long time. Therefore, it does not seem likely with any significant remaining tracer inside the borehole section prior to back-pumping. Diffusion of tracer into the rock along the borehole wall would be likely to occur, but the time period with high concentrations in the borehole is very short and the borehole wall area is relatively small (about 0.2–1.2 m^2).

During the recovery pumping, it is reasonable to assume a plug flow along the borehole in the 3 mm wide channel between the dummy and the borehole wall. The only possibility for any transient solute storage is diffusion through the borehole wall; i.e. when the peak of the breakthrough curve passes, solute diffuses into the rock and is then released later. However, based on supporting experimental data, a reasonable estimate of the maximum residence time in the borehole section during recovery pumping would be around one hour. With a slot width of 3 mm between dummy and borehole wall, and reasonable estimates of rock porosity and diffusivity, this would have negligible effect on the resulting recovery breakthrough curves.

4.4 Natural background flow though the borehole section

Immediately before each SWIW test, the ambient groundwater flow rate through the borehole section is determined from a tracer dilution test. If there is a large natural flow through the borehole, it may affect the shape of the recovery breakthrough curve. Such effects are simulated and discussed in /Nordqvist and Gustafsson 2002/. Results from dilution measurements for all of the SWIW tests are summarised in Table 4-1, where comparisons with experimental flow rates are made. For experiments where waiting phases occurred, the total flow through the section during the waiting phases is estimated based on the measured ambient background flow rate.

Table 4-1 shows that the natural flow rates through the borehole section generally only are a small fraction of injection and pumping flow rates during the SWIW tests. Although the flow rates are not directly comparable (the measured flow through the borehole section under natural conditions should be expected to flow through a smaller volume than the imposed flow during injection/pumping), the assumption made for the basic evaluation that natural gradients are not significant does not seem unreasonable. In KLX03 an exceptionally large natural flow rate was observed. If this flow rate would be representative for the entire fracture domain investigated by the SWIW test, natural flow might be expected to have a considerable impact on the SWIW recovery curves. However, such effects are not clearly indicated by the shape of the breakthrough curve. The simple advection-dispersion model fits both the ascending as well as most of the descending parts of the KLX03 curve well (as it does for other tests as well). Such a good fit to the descending part would probably not be obtained if a strong gradient had a significant effect. In addition, the tailing effect (at the later parts of the recovery curves) are observed for all tests, irrespective of the magnitude of the natural flow rate. There is no obvious pattern that high natural flow rates would cause more tailing in the Uranine breakthrough curves.

Table 4-1. Natural background flow through SWIW test sections from dilution measurements prior to each SWIW test.

Borehole	Section (m)	Natural flow (L/h)	SWIW injection flow (L/h)	SWIW pumping flow (L/h)	Total injected volume (L)	Natural flow volume during waiting phases (L)
KSH02	422.3–423.3	0.011	13–15[1]	15	204	0.03
KSH02	576.8–579.8	0.005	11.3–13	17.2	173.5	–
KLX03	740.4–744.4	0.253	12.9	13.9	312.4	0.17
KLX18A	473.3–476.3	0.002	2.4–2.9	2.5	111.1	–
KLX11A	516.5–519.5	0.031	18.0–18.6	18.2	98.5	–
KLX11A	598.0–599.0	0.001	9.2–9.7	9.4	95.3	–
KFM02A	414.7–417.7	0.0017	5.5–11.8	12.4	201	–
KFM03A	643.5–644.5	0.010	9.9	8.0	126.8	0.014
KFM08A	410.5–413.5	0.006	2.44	2.3	172.2	–
KFM04A	417.0–422.0	0.001	2.2–2.4	2.3	158.0	–
KFM01D	377.4–378.4	0.005	13.4–13.8	13.8	100.8	0.0025
KFM01D	431.0–432.0	0.010	3.8–4.2	3.8	101.4	0.001

[1] In this section, the borehole was open for almost 50 hours, resulting in an estimated outflow of water of 0.55 L/h.

5 Evaluation of SWIW tests with a matrix diffusion model

5.1 Simulation model

All of the SWIW tests performed within the site investigation programmes have been subject to a basic evaluation assuming homogenous radial flow and advective-dispersive transport, as described in chapter 3. An extended evaluation was carried out for section 422.3–423.3 m in KSH02 /Nordqvist 2007/, motivated by the observed lack of fit in the tails of the SWIW breakthrough curves. The results of the extended evaluation showed that the fit of the tail may be improved by assuming tracer exchange with immobile water. Herein, this evaluation model is employed to evaluate also all of the other performed SWIW tests within the SKB site investigation programmes. The simulation model used for all calculations is SUTRA /Voss 1984/.

The simulations including matrix diffusion are carried out assuming a vertical section with radial symmetry. The simulated geometry approximately corresponds to a dual-porosity approach based on the assumption of parallel fractures and is schematically illustrated in Figure 5-1. A similar approach was used by /Lessoff and Konikow 1997/ for simulation of SWIW tests. The previously described basic evaluation described in section 3.4 only included flow and transport in a single flowing fracture (or zone).

The simulation code is based on the finite-element method. The sizes of the elements should be carefully designed in order to obtain representative results. For these simulations, element sizes start very small closest to the borehole and expand with distance. The first element closest to the borehole is about 5 mm in the radial direction. In the vertical direction, the fracture is divided into ten elements (i.e. 0.01 mm each). In the matrix, element sizes increase with distance from the flowing fracture. There may be some discretisation effects at the narrow interface zone (the first elements in the matrix closest to the flowing fracture is 0.058 mm) where the fracture becomes the matrix. For strongly sorbing tracers, this interface zone may have some impact on the simulated results. In order to simulate an ideal dual-porosity system completely accurately, finer discretisation may be needed, although this would require much longer simulation times. The simulation mesh consists of 23,111 elements and 22,800 nodes.

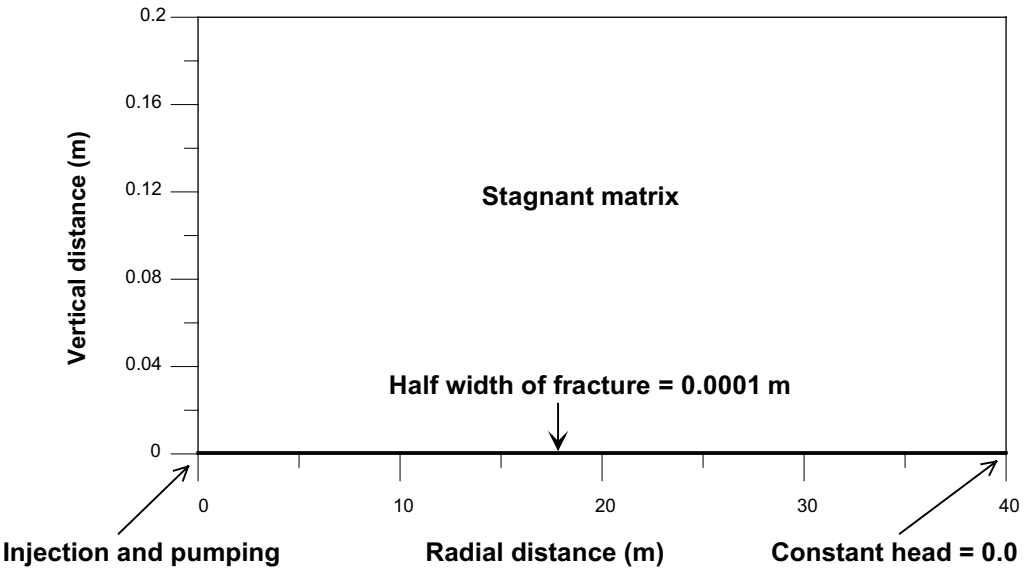

Figure 5-1. *Layout for simulation of SWIW test in a fracture with matrix diffusion.*

The solute transport is simulated with the standard advection-dispersion-diffusion model in two dimensions. The dispersion coefficients in the longitudinal (D_L) and transverse (D_T) directions, respectively, are commonly expressed by:

$$D_L = a_L v + D_m \quad (5\text{-}1a)$$

$$D_T = a_T v + D_m \quad (5\text{-}1b)$$

where a_L and a_T are the longitudinal and transverse dispersivities, respectively, v is the magnitude of the water velocity and D_m is the diffusion coefficient. In the radial cross-section in Figure 5-1, significant flow only takes place in the x-direction in the thin layer that represents the fracture and here the advective terms dominate. The transverse dispersivity has very little effect in this case, because all simulations are carried out in a cross section with radial symmetry.

In the stagnant matrix the diffusion term (D_m) dominates in equations 5-1a and 5-1b.

Some comments may be made here about dispersion in a SWIW experiment. The simulation model herein employs the traditional velocity-dependent dispersion model in porous media, which is commonly also adapted for flow and transport simulations in fractured media.

To what extent dispersion processes contribute to the shape of the recovery breakthrough curve in a SWIW experiment is not entirely clear. In a cross-hole tracer experiment, a large component of the dispersive effects is usually attributed to velocity variations among individual flow paths, which may be partly or fully independent, connecting the injection and sampling sections, respectively. In a SWIW experiment, this effect would not occur because of the flow reversibility. Tracers injected into fast as well as slow flow paths would return to the SWIW section at the same time, contrary to a cross-hole test.

In individual flow paths, which is here taken to mean a continuous flow domain of arbitrary dimension, some dispersive spreading would also be expected to occur. In laminar flow between two parallel plates, a parabolic cross-sectional velocity profile develops. Combined with molecular diffusion, this mechanism causes so called Taylor dispersion /Bodin et al. 2003a/. A thorough analysis of the effects of various forms of Taylor dispersion on SWIW tests in fractures is given by /Neretnieks 2007/.

Another mechanism that may add to dispersion is heterogeneity in fluid velocities within a flow path, caused by variation of fracture aperture and/or fracture roughness. In this case, the dispersive effect depends on the geometrical characteristics of the fracture plane within the flow path.

These dispersion mechanisms would be expected to occur simultaneously and not be reversible during a SWIW experiment. Thus, some dispersive effects would be expected to influence the recovery curve in a SWIW tests, although the effect would be expected to be smaller than in cross-hole tracer experiments. It may be mentioned that /Becker and Shapiro 2003/ consider heterogeneous advection in multiple flow paths that gives effects on SWIW recovery curves because of different dispersion characteristics within each flow path.

In the simulation models used herein, dispersion is represented with a longitudinal dispersion coefficient that is proportional (the proportionality constant being the longitudinal dispersivity) to the water velocity. In radial flow geometries, the velocity varies considerably with distance unlike in one-dimensional flow geometries where the velocity usually is assumed to be constant along the flow path. Although this assumption of a linear dependence of the dispersion coefficient on velocity commonly is employed also for SWIW tests in fractured rock /e.g. Becker and Shapiro 2003, Altman et al. 2002, Haggerty et al. 2001/, one should be aware of that alternative descriptions of dispersion mechanisms are possible /Neretnieks 2007/. Nevertheless, the combined effects of Taylor dispersion and aperture variations results in a complex dispersion that affects tracer recovery in a SWIW test.

The layout in Figure 5-1 represents a single plane-parallel fracture with an assumed width of 0.0002 m (half width = 0.0001 m) having a porosity of 1.0. The stagnant matrix (simulated with a very low value of hydraulic conductivity) extends, on both sides of the fracture, to a distance

of 0.2 m away from the centre of the fracture. The model extends 40 m in the radial direction, which is intended to be well beyond the distances that solute may travel during the fluid injection phases employed in the evaluated SWIW tests. A porosity value is assigned to the stagnant matrix (p_m) as well as a pore diffusivity value. The latter is less than diffusivity in water due to tortuosity and constrictivity effects. The pore diffusivity, D_p [L^2/T], is commonly defined as /Bodin et al. 2003b/:

$$D_p = D_W \frac{\delta_D}{\tau^2} \tag{5-2}$$

where D_W is the diffusivity in free water [L^2/T], δ_D is the constrictivity [–] and τ^2 is the tortuosity [–].

Sorption of tracers is in this case considered only for the stagnant matrix, which is different fram the basic evaluation where only sorption in the flowing fracture was considered.

Sorption in the matrix is simulated assuming linear equilibrium sorption (K_d-sorption). One-dimensional transport of a sorbing tracer by diffusion may be described by:

$$\frac{\partial C_m}{\partial t} = \frac{D_p}{R_m} \frac{\partial^2 C_m}{\partial z^2} \tag{5-3}$$

where C_m is solute concentration in the matrix [M/L^3], D_p is the pore diffusivity [L^2/T]. The matrix retardation factor, R_m, is given by:

$$R_m = 1 + \frac{\rho_s (1 - p_m)}{p_m} K_d \tag{5-4}$$

where ρ_s is the density of the solid [M/L^3], p_m is the matrix porosity [–] and K_d is the distribution coefficient for linear equilibrium sorption [L^3/M].

In the simulations herein with SUTRA, however, diffusion in the matrix is not strictly one-dimensional because the employed model is fully two-dimensional throughout the simulation domain.

Non-linear regression was used to fit the simulation model to experimental data. Simultaneous fitting of both tracer breakthrough curves (Uranine and cesium), and calculation of fitting statistics, was carried out using the same basic approach as in the previous evaluations of SWIW tests within the site investigation programmes (see for example /Gustafsson and Nordqvist 2005/), which is basically based on the Marquardt method for weighted non-linear regression /Marquardt 1963/. In some cases sequential estimation was employed instead, i.e. Uranine was fitted first to obtain parameters for a non-sorbing tracer (a_L, p_m) and then K_d for the sorbing tracer was determined in a second regression run with other parameters fixed from the first run. Other variants that sometimes were used include varying the assignment of regression weights in order to emphasize certain parts of the experimental data in the fitting procedure. The variations in the fitting procedure is only a practical matter in order to better and more rapidly obtain good fits between experimental data and simulations.

A complete list of the various SUTRA model parameters that influence the computed breakthrough curve in the simulation model employed includes:

- fracture aperture,
- longitudinal dispersivity,
- matrix porosity,
- tracer diffusivity,
- solid density,
- linear sorption coefficient (K_d).

In addition, the total injected volume also influences the dispersion as described in section 3.3.

The listed parameters may not all be determined independently from SWIW breakthrough curves. Instead, groups of combined parameters effectively determine the shape of the breakthrough curve. For example, the dispersion effect is governed by a combination of longitudinal dispersivity, fracture aperture and the total injected volume as described in section 3.3. Further, the matrix diffusion effect for a non-sorbing tracer (i.e. Uranine) may be combined into a group using /Moreno et al. 1983/:

$$A = \frac{\delta}{2p_m\sqrt{D_p}} \tag{5-5}$$

where δ is the fracture aperture [L].

For a sorbing tracer the combined parameter above extends to:

$$A_R = \frac{\delta}{2p_m\sqrt{R_m D_p}} \tag{5-6}$$

If a non-sorbing tracer is fitted simultaneously with a sorbing tracer, some further simplifications may be made under certain assumptions and a value of the matrix retardation factor (R_m) may be estimated. This may be explained by the following reasoning. If one assumes that both of the tracers "experience" the same aperture, matrix porosity and tortuosity/constrictivity and that the ratio of the diffusion coefficients for the two tracers in water is known, then R_m may be obtained from:

$$R_m = \frac{D_W}{D_{W,R}}\left(\frac{A}{A_R}\right)^2 \tag{5-7}$$

where D_W and $D_{W,R}$ denotes the diffusion coefficients for the non-sorbing and sorbing tracers, respectively.

The assumption that all the formation parameters are the same for both of the tracers is, of course, only strictly valid for a homogenous system (i.e. a homogenous fracture with a homogenous matrix), because the non-sorbing tracer reach farther into the formation than the sorbing tracer. In the results section (section 5.2), the estimated parameters are presented as A and R_m, the latter based on the assumption of a value of 5 for the cesium/Uranine water diffusivity ratio.

In practise, the SUTRA simulation model does not explicitly use the effective parameters A and R_m as input. Instead, the dispersivity, matrix porosity and the matrix K_d are estimated with fixed values (see above) of fracture aperture, tracer diffusivities and solid density. Based on this, A and R_m are calculated from equations 5-6 and 5-4, respectively.

5.2 Results

In this section, evaluations with the matrix diffusion model for each SWIW test are shown. Brief comments for each test section are given for each plotted figure showing the fit between model and experimental data. A summary of simulation results and further overall discussion is then given in section 5.3.

Estimated parameters are presented as the effective matrix diffusion parameter (A) and the matrix retardation factor (R_m) as discussed in the preceding section. In addition, the effective dispersion parameter (τ) is given (see equation 3-2). Note that for some of the regression runs, the retardation factor approached very large values and for those cases only a judged lower limit is given.

Only one of the sorbing tracers, cesium, is evaluated here. Rubidium was not used in all of the tests, and the resulting experimental data are very similar to those of cesium.

5.2.1 KSH02 section 422.3–423.3 m

The best-fit estimate of Uranine and cesium is shown in Figure 5-2. A very high retardation effect for cesium is indicated. The model fit to experimental data is fairly good and improved (for both of the tracers) compared with the advection-dispersion model.

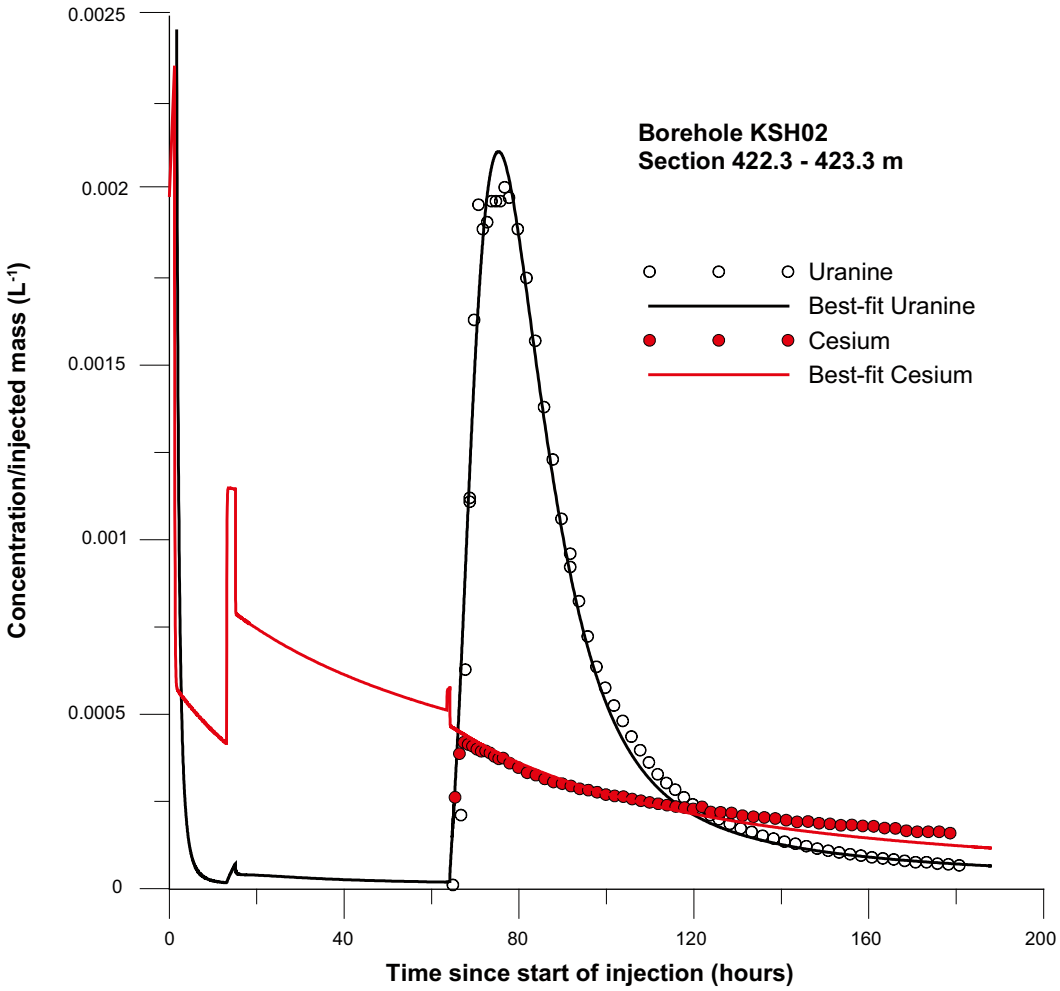

Figure 5-2. *Simultaneous fit of Uranine and cesium data in KSH02, section 422.3–423.3 m . Estimated parameter values: $A = 400$, $R_m > 10^4$, $\tau = 0.4$.*

5.2.2 KSH02 section 576.8–579.8 m

The best-fit estimate of Uranine and cesium is shown in Figure 5-3. Compared with section 422.3–423.3 m in the same borehole, the retardation effect for cesium is more moderate. The model fit to experimental data is fairly good and the Uranine fit is improved compared with the advection-dispersion model. The cesium fit is in this case similar to the case with the advection-dispersion model.

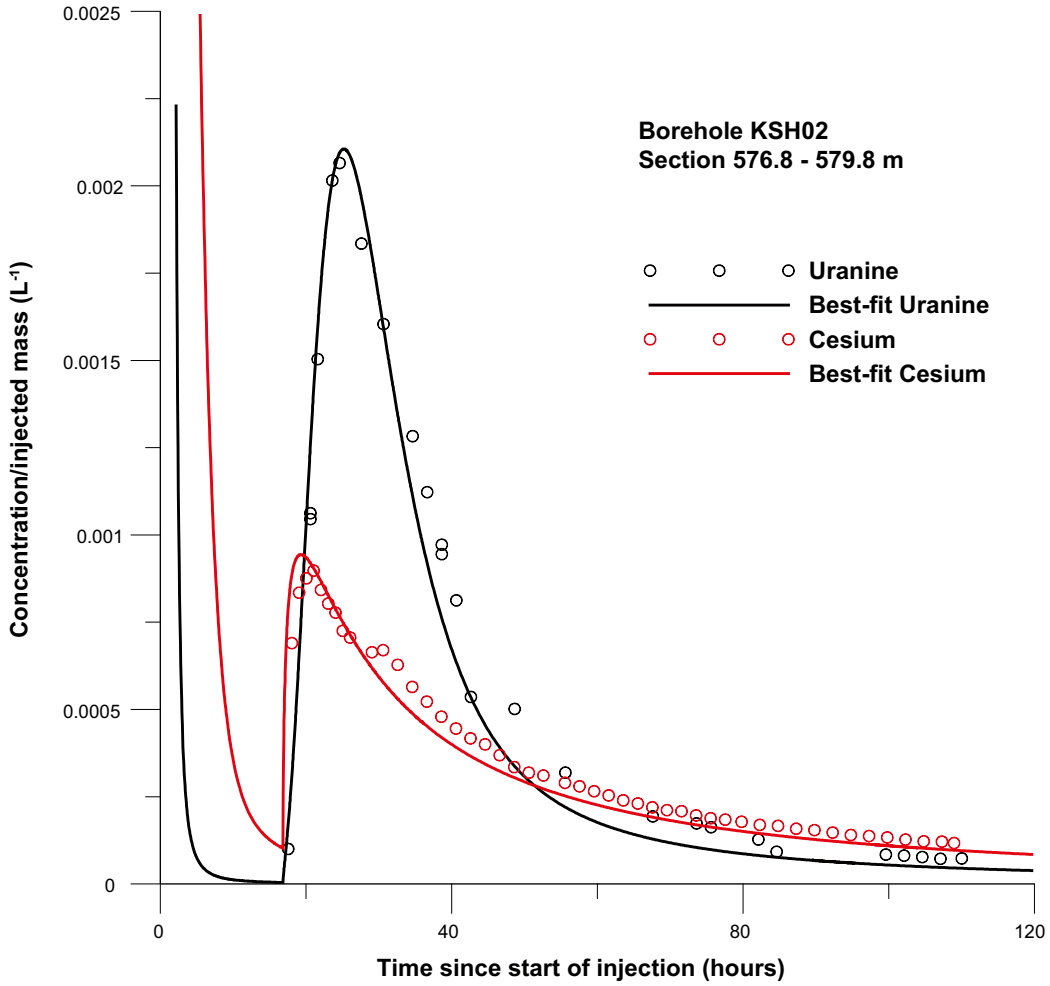

Figure 5-3. *Simultaneous fit of Uranine and cesium data in KSH02, section 576.8–579.8 m. Estimated parameter values: A = 370, R_m = 118, τ = 0.7.*

5.2.3 KLX03 section 740.4–744.4 m

The best-fit estimate of Uranine and cesium is shown in Figure 5-4. The model fit to experimental data for Uranine is fairly good and better compared with the advection-dispersion model. A very high retardation effect for cesium is indicated. The model fit for cesium is not entirely satisfactory, especially at the beginning of the cesium curve. In this case, it appears that the fit for cesium is somewhat better using the advection-dispersion model (Figure 3-3).

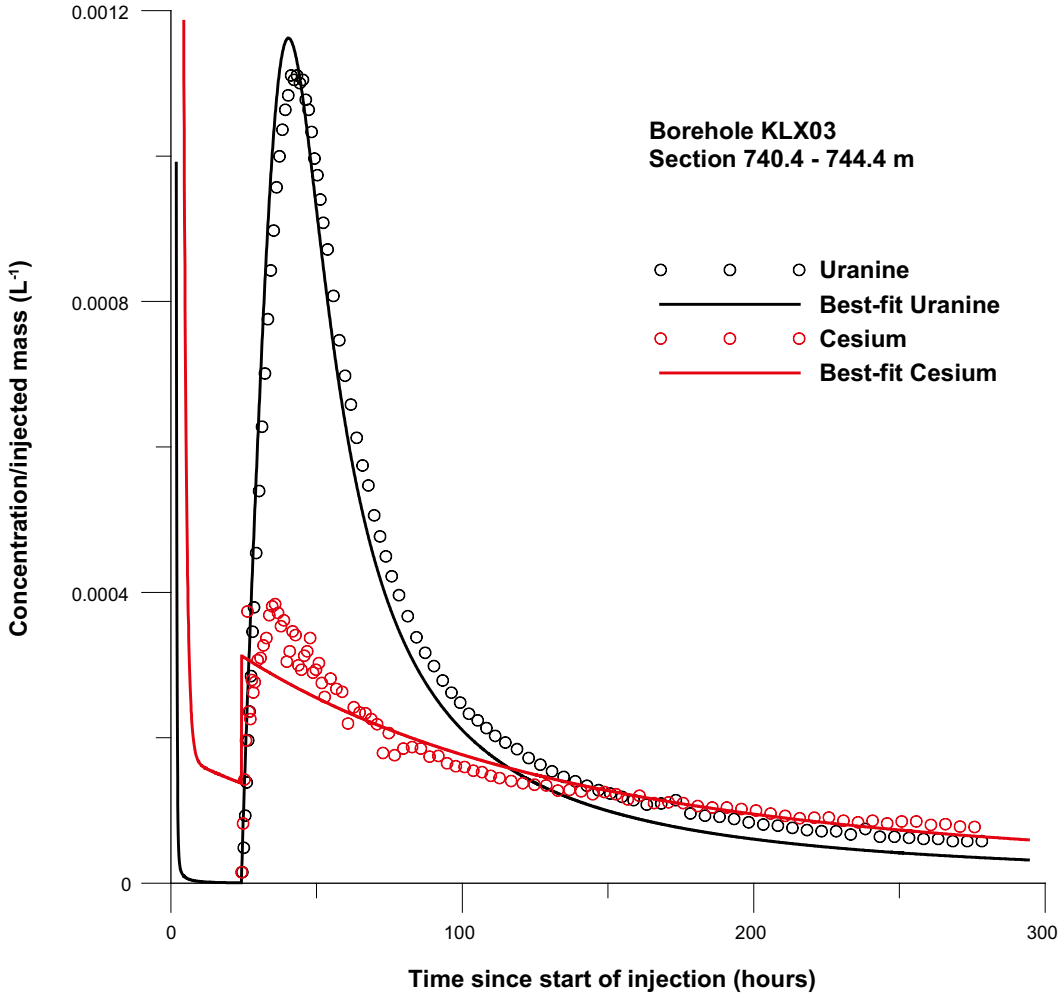

Figure 5-4. *Simultaneous fit of Uranine and cesium data in KLX03, section 740.4–744.4 m. Estimated parameter values: $A = 143$, $R_m > 10^4$, $\tau = 0.04$.*

5.2.4 KLX18A section 473.3–476.3 m

The best-fit estimate of Uranine and cesium is shown in Figure 5-5. The model fit to experimental data for Uranine is fairly good and better compared with the advection-dispersion model. A very high retardation effect for cesium is indicated. However, the model fit for cesium is not entirely satisfactory. In this case, it appears that the fit for cesium is fitted significantly better using the advection-dispersion model (Figure 3-3).

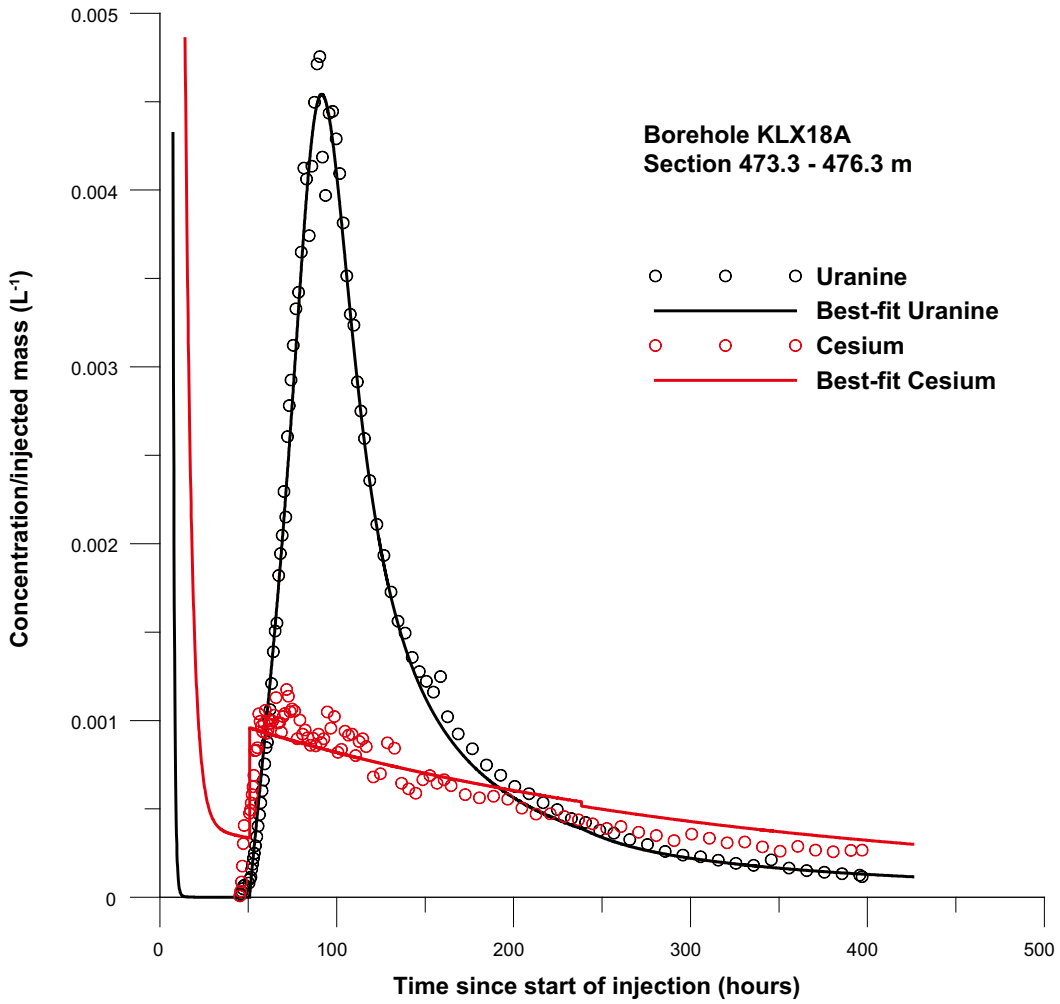

Figure 5-5. *Simultaneous fit of Uranine and cesium data in KLX18A, section 473.3–476.3 m. Estimated parameter values: $A = 323$, $R_m > 10^4$, $\tau = 0.1$.*

5.2.5 KLX11A section 516.5–519.5 m

The best-fit estimate of Uranine and cesium is shown in Figure 5-6. The model fit to experimental data for Uranine is fairly good and better compared with the advection-dispersion model. A very high retardation effect for cesium is indicated. The model fit for cesium is not satisfactory and a significantly better fit for cesium is obtained with the advection-dispersion model (Figure 3-3).

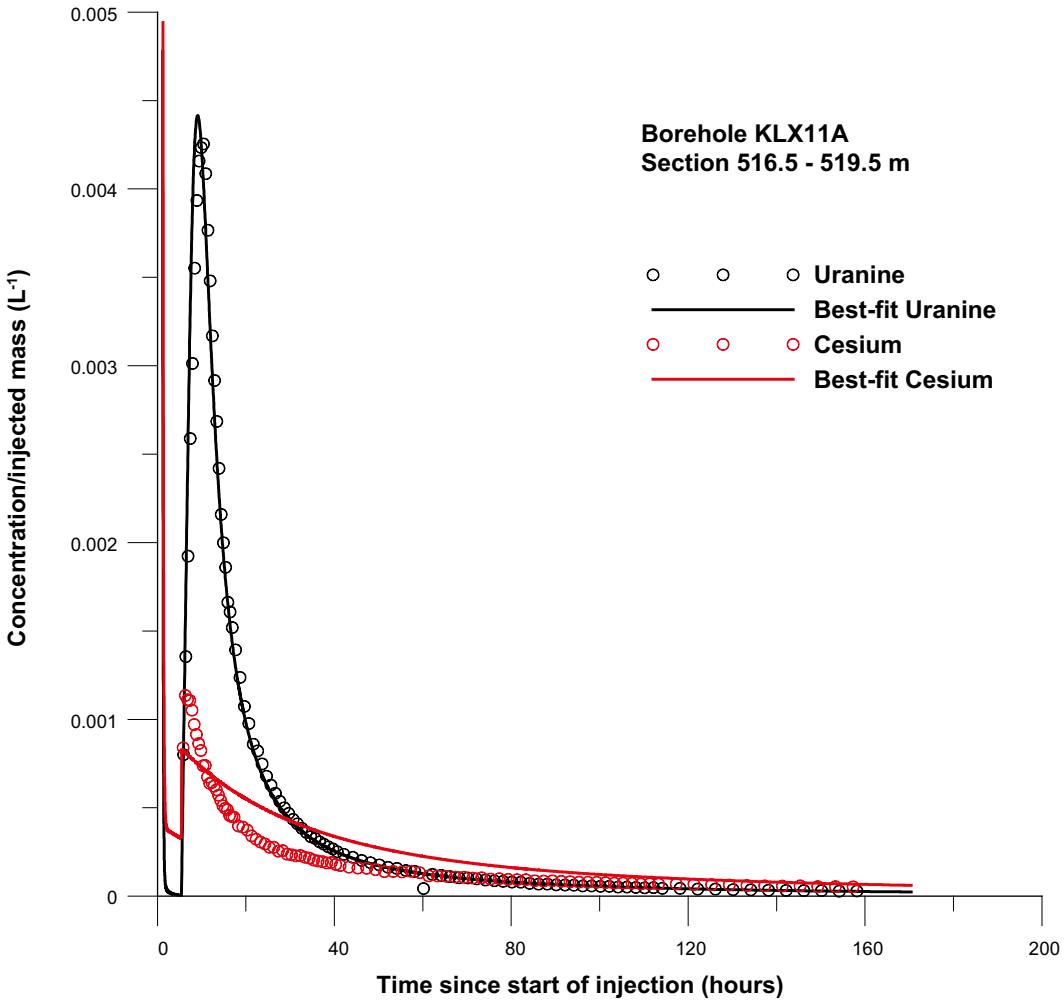

Figure 5-6. *Simultaneous fit of Uranine and cesium data in KLX11A, section 516.5–519.5 m. Estimated parameter values: $A = 86$, $R_m > 10^4$, $\tau = 0.1$.*

5.2.6 KLX11A section 598.0–599.0 m

The best-fit estimate of Uranine and cesium is shown in Figure 5-7. The model fit to experimental data is fairly good for Uranine and better compared with the advection-dispersion model. The fit to cesium is not entirely satisfactory and it could be argued that the fit to cesium is somewhat better with the advection-dispersion model (Figure 3-3).

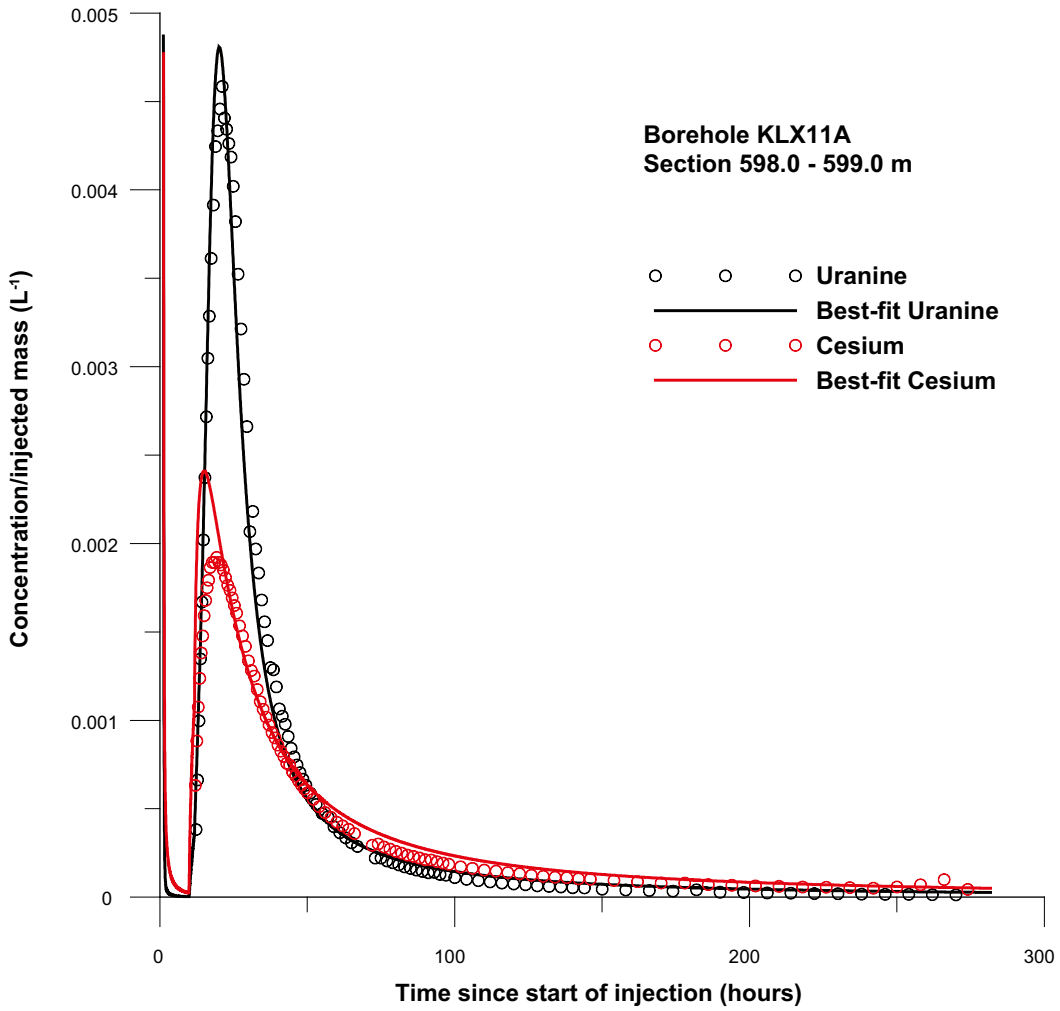

Figure 5-7. *Simultaneous fit of Uranine and cesium data in KLX11A, section 598.0–599.0 m. Estimated parameter values: A = 182, R_m = 12.8, τ = 0.09.*

5.2.7 KFM02A section 414.7–417.7 m

The best-fit estimate of Uranine and cesium is shown in Figure 5-8. The model fit to experimental data is fairly good and the fits for both of the tracers are improved compared with the advection-dispersion model. The model fit results in an unusually low value of the matrix retardation factor of about 1.6.

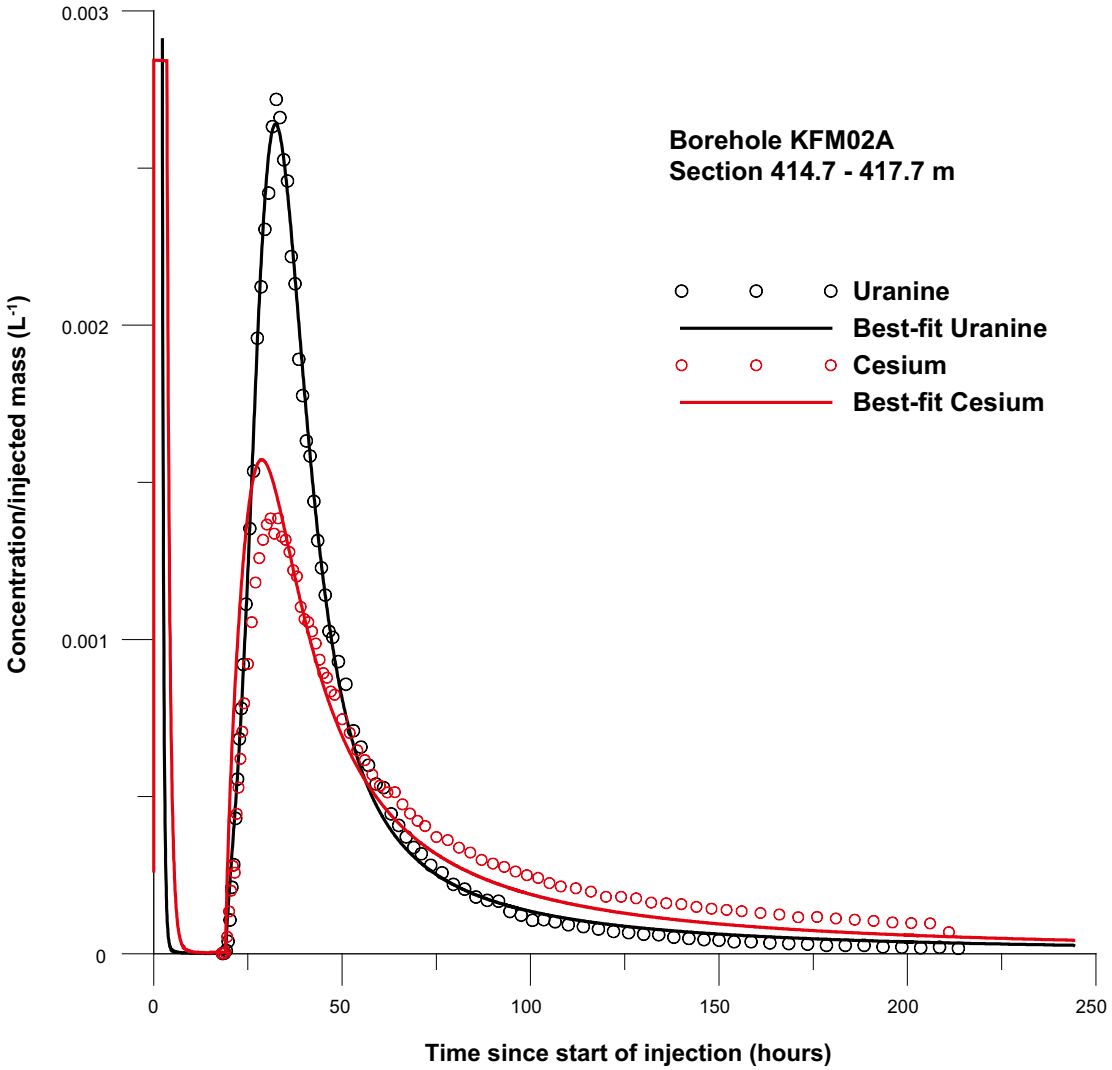

Figure 5-8. *Simultaneous fit of Uranine and cesium data in KFM02A, section 414.7–417.7 m Estimated parameter values: A = 282, R_m = 1.6, τ = 0.09.*

5.2.8 KFM03A section 643.5–644.5 m

The best-fit estimate of Uranine and cesium is shown in Figure 5-9. The model fit to experimental data is fairly good and the fits for both of the tracers are improved compared with the advection-dispersion model. The estimated dispersion parameter is unusually high compared with other tests; this was also the case for the basic evaluation with the advection-dispersion model (Table 3-5).

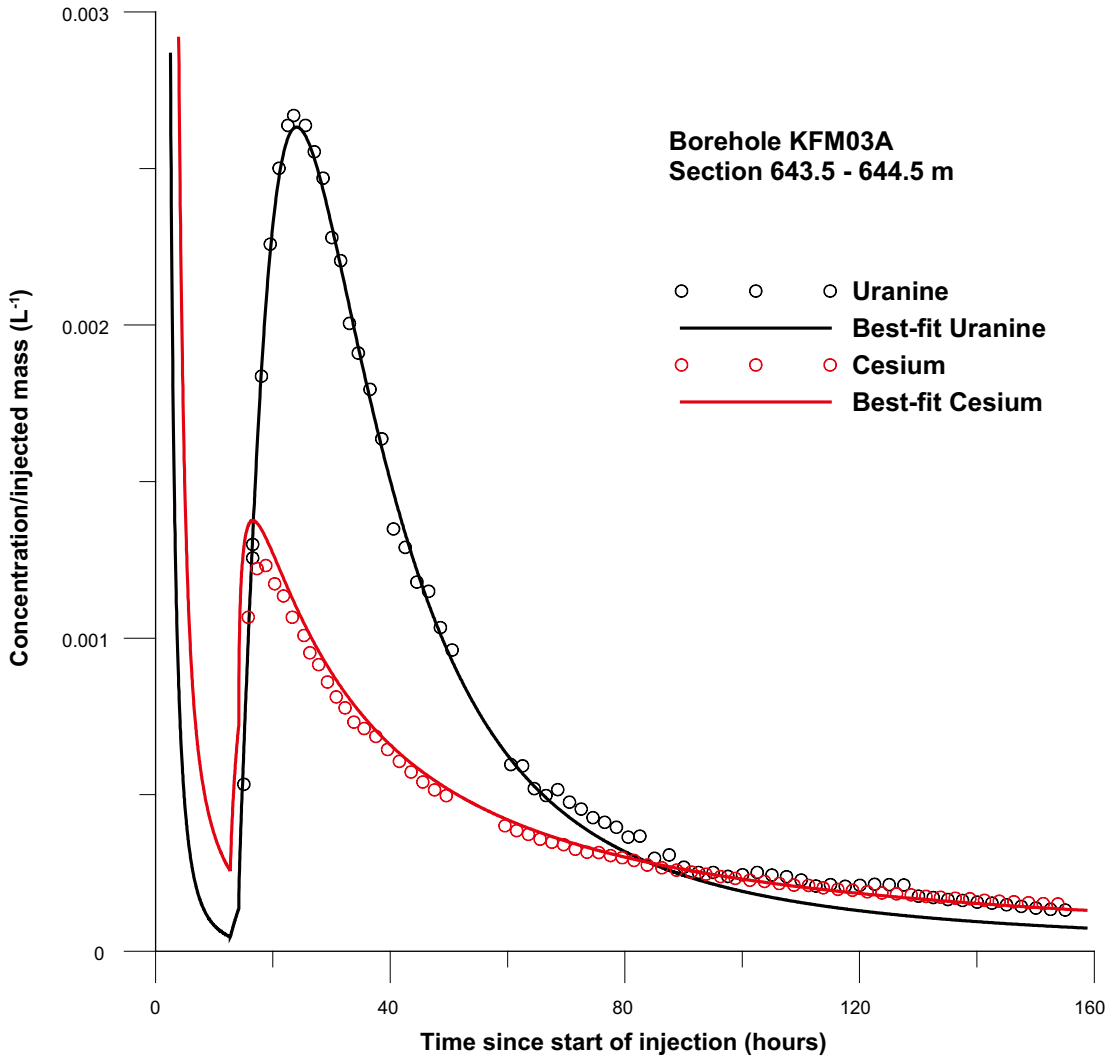

Figure 5-9. *Simultaneous fit of Uranine and cesium data in KFM03A, section 643.5–644.5 m Estimated parameter values: A = 377, R_m = 426, τ = 2.7.*

5.2.9 KFM08A section 410.5–410.5 m

The best-fit estimate of Uranine is shown in Figure 5-10. The model fit to experimental data for Uranine is fairly good and better compared with the advection-dispersion model. Because of previous evaluation problems when simultaneous fitting of Uranine and sorbing tracers from this test /Gustafsson et al. 2006b/, cesium was not evaluated in this case.

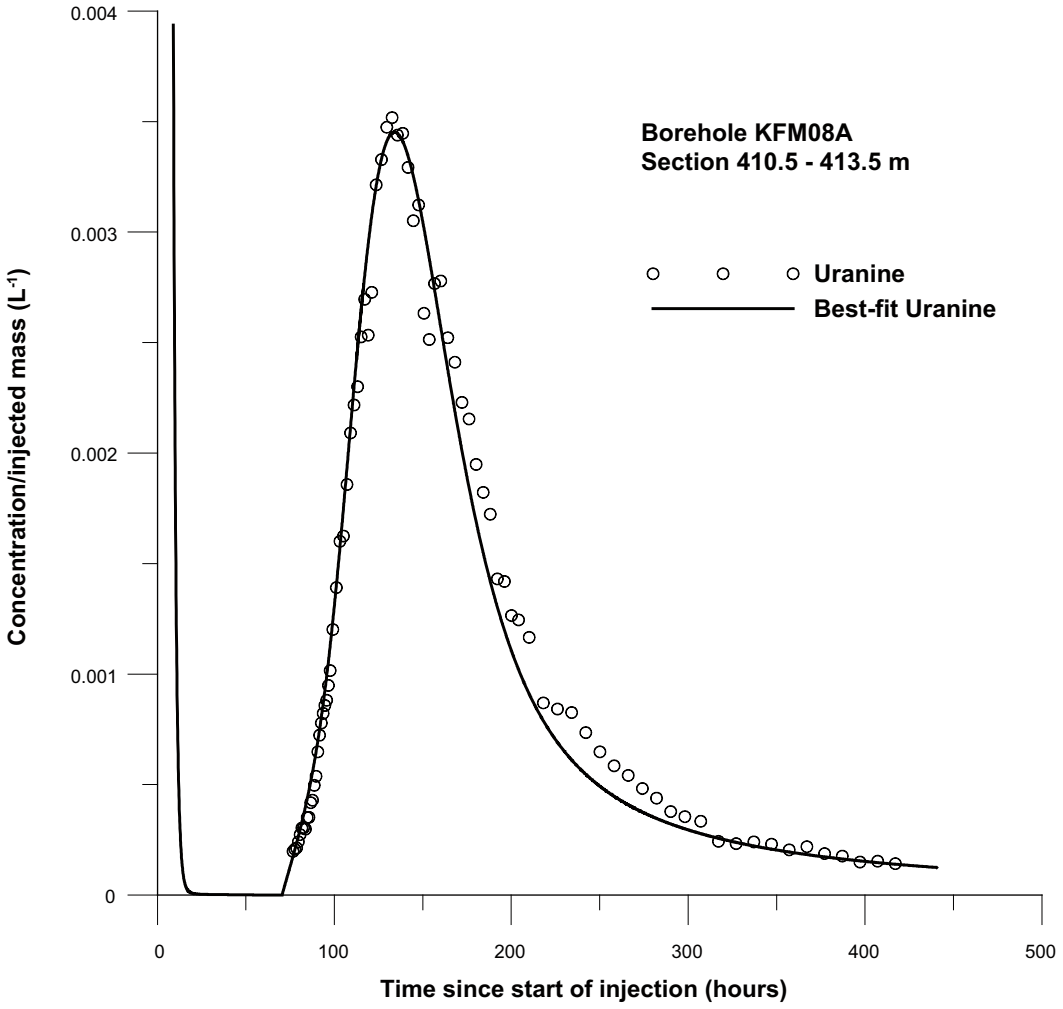

Figure 5-10. *Fit of Uranine data in KFM08A, section 410.5–413.5 m. Estimated parameter values: $A = 741$, $\tau = 0.08$.*

5.2.10 KFM04A section 417.0–422.0 m

This test was not evaluated because of unusually low Uranine recovery /Gustafsson et al. 2006c/. There is some evidence that Uranine, during the injection and chaser phases, may have been pushed back into the borehole (but outside the test section) through connected fractures.

5.2.11 KFM01D section 377.4–378.4 m

The best-fit estimate of Uranine and cesium is shown in Figure 5-11. The model fit to experimental data is fairly good and better (for cesium only slightly better) compared with the advection-dispersion model.

5.2.12 KFM01D section 431.0–432.0 m

The best-fit estimate of Uranine and cesium is shown in Figure 5-12. The model fit to experimental data is fairly good and better (for cesium only slightly better) compared with the advection-dispersion model. The results from this section are very similar to the other tested section (see preceding test) in this borehole.

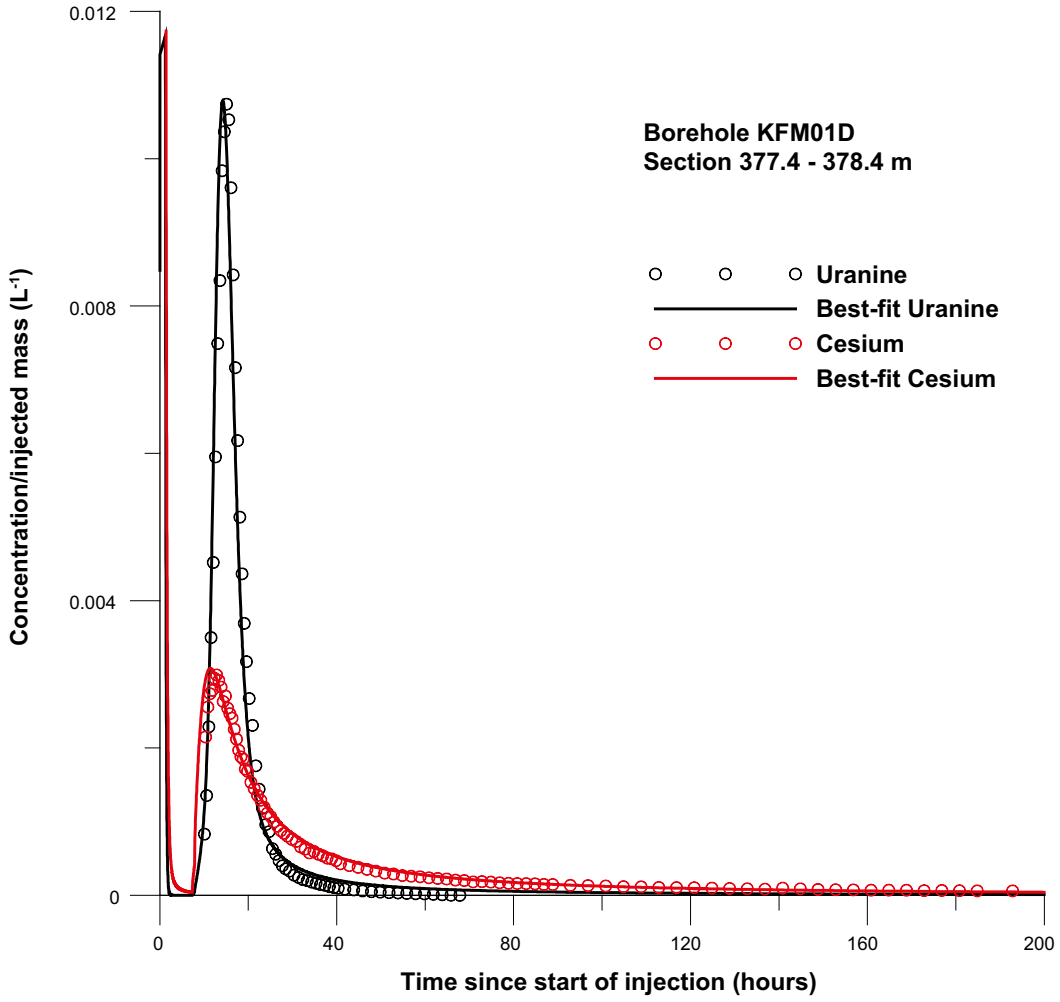

Figure 5-11. *Simultaneous fit of Uranine and cesium data in KFM01D, section 377.4–378.4 m. Estimated parameter values: A = 382, R_m = 1,890, τ = 0.05.*

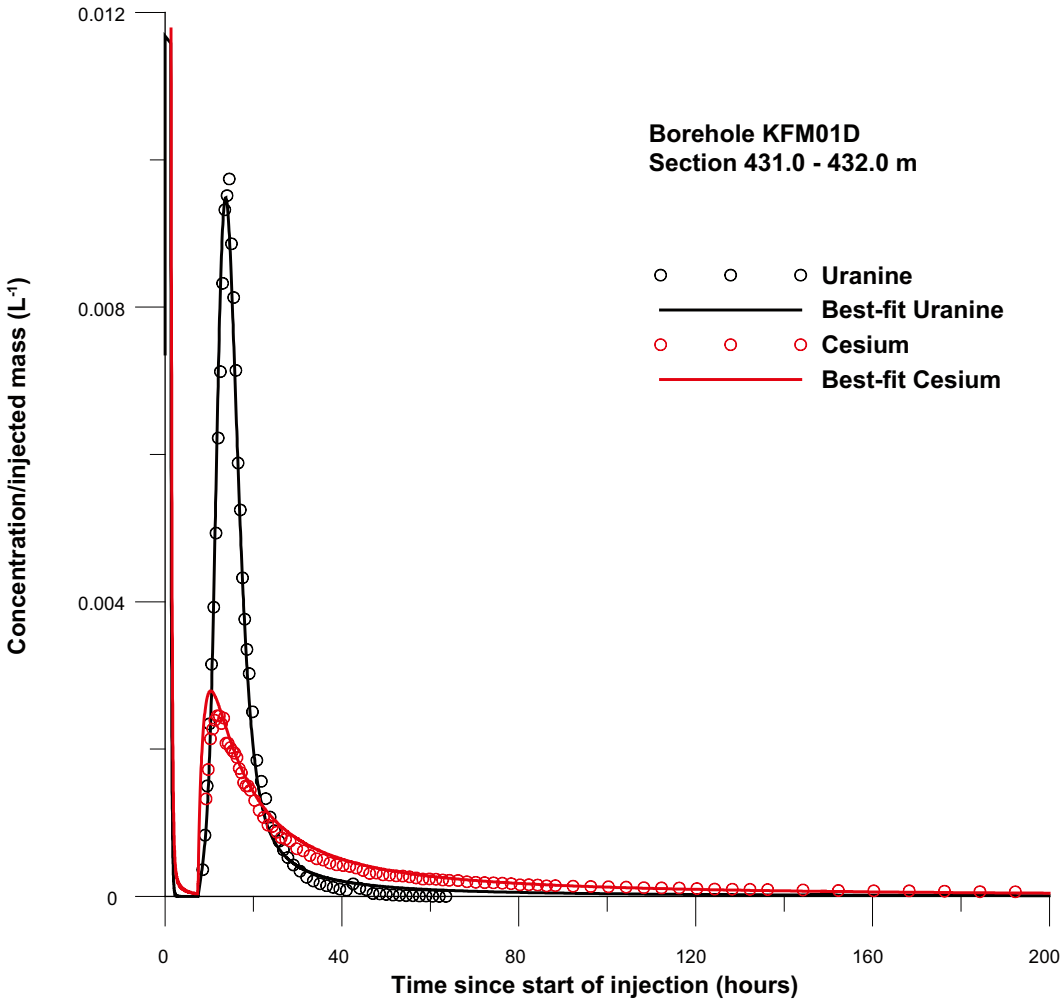

Figure 5-12. *Simultaneous fit of Uranine and cesium data in KFM01D, section 431.0–432.0 m. Estimated parameter values: A = 420, R_m = 530, τ = 0.03.*

5.3 Summary of simulations with the matrix diffusion model

A summary of all of the simulated SWIW tests using the matrix diffusion model is presented in Table 5-1. The effective parameters R_m (matrix retardation factor for Cs, equation 5-4) and the diffusion parameter A (equation 5-5) for Uranine are given in the table along with the dimensionless dispersion parameter (equation 3-2). The table also shows the fracture retardation factor obtained with the advection-dispersion model (also listed in Table 3-5) for comparison.

An overall assessment of the fits of the experimental SWIW data using the matrix diffusion model is that, in all of the simulated cases, the observed tailing in the Uranine curves are fitted well, in contrast to the fits obtained with the advection-dispersion model. This is a consistent difference between the two model evaluation approaches. For the sorbing tracers, however, the result is much less consistent. In some of the cases, the fit for the cesium data using the advection-dispersion model is equal or better than for the matrix diffusion model. This appears to be the case especially for the more strongly sorbing cases, for which the matrix diffusion model often give relatively poor fits. One hypothetical explanation for this is that the simpler advection-disperion model with sorption only on fracture surfaces is sufficient for this sorption behaviour. It would be possible to include sorption in the flowing fracture as well in the matrix diffusion simulation model. However, this would add substantially to the complexity of the evaluation and has not been considered here.

Table 5-1. Estimation results with the matrix diffusion model. The retardation factors for Cs obtained with the advection-dispersion model (see section 3-4) are also included for comparison.

Borehole	Section (m)	a_L^2 δ/Vinj×10^{-3}	A ($s^{1/2}$) (Uranine)	Rm (Cesium)	R (AD-model) (Cesium)
KSH02	422.3–423.3	0.4	400	> 10^4	975
KSH02	576.8–576.9	0.7	370	118	87
KLX03	740.4–744.4	0.04	143	> 10^4	235
KLX18A	473.3–476.3	0.1	323	> 10^4	857
KLX11A	516.5–519.5	0.1	86	> 10^4	808
KLX11A	598.0–599.0	0.09	182	12.8	66
KFM02A	414.7–417.7	0.09	282	1.6	11
KFM03A	643.5–644.5	2.7	377	426	73
KFM08A[1)]	410.5–413.5	0.08	741	–	34
KFM04A[2)]	417.0–422.0	–	–	–	–
KFM01D	377.4–378.4	0.05	382	1,890	535
KFM01D	431.0–432.0	0.03	420	530	918

[1)] This section was only partly evaluated because of possible ambiguity regarding Uranine concentrations /Gustafsson et al. 2006b/ and values may be uncertain.

[2)] This section was not evaluated because of incomplete Uranine recovery.

The estimated values for the matrix diffusion parameter, A, for Uranine show fairly moderate variation among the tested borehole sections. The estimated values are typically in the range of 100–400 $s^{½}$, except for one anomalously large value (741) for KFM08A. The values of A indicate a relatively large matrix diffusion effect compared with what might be expected from typical literature data /Liu et al. 2006/. One possible explanation for such high diffusion effects may be that diffusion to a large extent occurs into stagnant water adjacent to the flowing channels rather than into the rock matrix.

The range of the estimated retardation factor for cesium in the rock matrix is very large. An examination of the resulting matrix retardation factors shows that many of the tests give moderate values but also that some tests result in very high values. Because the tests with the highest R_m-values generally show the poorest fit for cesium (with the exception of KSH02, section 422.3–423.3 m), it may be reasonable to question those retardation factors more than from tests with the more moderate values. Further, with such strong retardation there may also be effects of the finite element discretisation at the fracture/matrix boundary. One reasonable way to view those results might to consider the values as "large". It may be noted, however, that available laboratory data (/Byegård et al. 2006b/, Byegård pers. comm.) for the matrix rock porosity and K_d-values at Laxemar and Forsmark also indicate matrix retardation factors on the order of 10^3 or higher.

One of the tests, KFM02A section 414.7–417.7 m, results in a very small matrix retardation factor of about 1.6. This is consistent with the results using the advection-dispersion model which clearly resulted in the lowest fracture retardation factor among the tests. A recent cross-hole test with this section as injection section has also indicated rather moderate retardation for cesium /Lindquist et al. 2007/.

A comparison between the matrix retardation values obtained with the matrix diffusion model and the fracture retardation values obtained with the advection-dispersion model indicates that high values for one model also corresponds approximately to high values for the other model, and vice versa for low values. It should be noted that the retardation coefficents for the two simulation models (advection-dispersion and matrix diffusion, respectively) are not directly comparable. The matrix diffusion model only contains a retardation factor for the matrix but not for the flowing fracture, and the total retardation effect in the flowing fracture comes from a combination of

matrix diffusion and matrix retardation. Thus, retardation factors may be compared for borehole sections for each model, but not necessarily between models for a given borehole section.

The dispersion parameter shows generally much lower values than for the advection-dispersion model, which may be expected because the added process of matrix diffusion would be expected to account for some of the apparent dispersion effect. The exception to this is for the SWIW test in KFM03A, which shows anomalously large values of the dispersion parameter for both evaluation approaches.

It is difficult to identify any clear correlation between rock characteristics (Tables 3-2 and 3-3) and the results in Table 6-1, except in a few cases. For example, the clearly lowest retardation of cesium is found in KFM02A, which is consistent with the fact that no fracture minerals are found in this section. This is also the only SWIW tests section without fracture minerals. Further, the smallest matrix diffusion effect (i.e. the highest value of A) is found in KFM08A, which is characterized as a single fracture with a fresh fracture surface and a smooth laminar surface.

A possible influence of water chemistry characteristics may be indicated in KLX11A, where the uppermost section (516.5–519.5 m) is located in fresh water (89 mg/L chloride) and where section 598.0–599.0 is located in saline water (1,040 mg/L chloride). The section with fresh water here shows a significantly larger retardation effect than the section with saline water, which is consistent with what would be expected from water chemistry considerations alone. However, other fracture characteristics also differ somewhat between these two sections. The section in KLX11A with fresh water is the only one among all the SWIW test sections with fresh water.

A comparison of results between sites is somewhat limited by the fact that one of the Forsmark tests (KFM04A) was not evaluated and another one (KFM08A) only partly evaluated. However, there may be a tendency to find higher retardation factors in Oskarshamn, although there are moderately low values there as well. However, there are too few tests to suggest that this is a significant difference between the sites.

The magnitude of the values of parameter A may be considered typical for what is obtained in cross-hole tests, see for example /Moreno et al. 1983, Andersson et al. 2004/. It is generally recognized that the values of A indicate much larger diffusion effect than would be predicted from laboratory measurements of matrix porosity and diffusivity.

In order to illustrate how the values of A relate to other independent data, a theoretical fracture aperture is calculated for each test and listed in Table 5-2. The calculation of aperture from A obtained from the matrix diffusion model evaluation is based on formation factor values determined in situ, obtained from the SICADA data base. The formation factor, F, is defined as /Löfgren and Neretnieks 2002/:

$$F = \frac{D_e}{D_w} \tag{5-8}$$

where D_e [L^2/T] is the effective diffusivity (= $p_m D_p$). Combining 5-8 with 5-5 and re-arranging, one may calculate the aperture from:

$$\delta = 2A\sqrt{p_m F D_W} \tag{5-9}$$

The measured formation factor values for the SWIW test sections range approximately between 1×10^{-5} to 5×10^{-4}. No data is presently available for KLX11A and KLX18A and a value of 1×10^{-4} has been assumed for those sections. Reported values for determined matrix porosity values do not vary substantially /Byegård et al. 2006ab/ and a typical value of 0.25% is assumed. In addition, values for a magnitude larger porosity is also included in Table 5-2. The value for diffusivity in water for Uranine is assumed to be 5×10^{-10} m^2/s. Finally, the table includes aperture values calculated according to the cubic law, based on the transmissivity in each section (Table 3-1). The cubic law relates the transmissivity to the fracture aperture in a smooth planar fracture with parallel fracture walls and calculated apertures may thus be regarded as a lower bound for the aperture.

Table 5-2. Apertures calculated from the cubic law and from values of A obtained from the model evaluation with the matrix diffusion model.

Borehole	Section (m)	Aperture from cubic law (m)	Aperture from A (m) p_m = 0.0025	Aperture from A (m) p_m = 0.025
KSH02	422.3–423.3	1.17E–04	7.10E–06	2.24E–05
KSH02	576.9–579.8	9.39E–05	1.14E–05	3.61E–05
KLX03	740.4–744.4	1.85e–04	6.71E–06	2.12E–05
KLX18A	473.3–476.3	4.09E–05	7.22E–06	2.28E–05
KLX11A	516.5–519.5	1.75E–04	1.92E–06	6.08E–06
KLX11A	598.0–599.0	6.06E–05	4.07E–06	1.29E–05
KFM02A	414.7–417.7	1.15E–04	6.05E–06	1.91E–05
KFM03A	643.5–644.5	1.58E–04	8.76E–06	2.77E–05
KFM08A	410.5–413.5	2.51e–05	1.60E–05	5.07E–05
KFM04A	417.0–422.0	2.42E–05	–	–
KFM01D	377.4–378.4	7.98E–05	5.23E–06	1.65E–05
KFM01D	431.0–432.0	1.17E–04	4.79E–06	1.51E–05

The cubic law relates the transmissivity, T, to fracture aperture, δ, in a parallel-plate fracture with smooth laminar flow by:

$$T = \frac{\rho g}{12\mu}\delta^3 \qquad (5\text{-}10)$$

where r is the water density [M/L^3], m is the dynamic viscosity [$ML^{-1}T^{-1}$] and g is the gravitational acceleration [L/T^2].

The aperture values calculated from estimated values of the A parameter, and based on other assumptions as described above, are very small and considerably smaller than the theoretical lower bound represented by the cubic law apertures. This is the case irrespective of whether the tested section is considered to consist of a single flowing fracture or several flowing fractures.

The aperture example calculations imply that the estimated values of A require higher values of the formation factor than has been measured in situ. For typical porosity values for matrix rock (2.5×10^{-3}), calculated apertures values are about a magnitude lower than corresponding values calculated with the cubic law, the only exception being KFM08A. For an assumed higher porosity value of 0.025, the calculated apertures values are typically several times lower.

In Table 5-3, as an alternative comparison, formation factor values measured in boreholes (obtained from the SICADA data base) are compared with corresponding values calculated from estimated A values, cubic law aperture values and an assumed porosity value of 0.025. With the exception of borehole KFM08A, the formation factor values calculated from estimated A values are considerably higher than the measured ones for the corresponding SWIW test sections.

It is apparent from the comparisons of estimated A values and other independent data that the matrix diffusion effects in the SWIW tests seem to be considerably larger than what be expected from independent data, which may be considered a typical result for field tracer tests in general. Some possible explanations to this may be due to the simplistic nature of the employed simulation model. For example, available surfaces for diffusion may be considerably larger than in the assumed parallel smooth fracture assumed in the simulation model. Diffusion may also occur into non-flowing water volumes in the fracture, which would result in relatively fast diffusion compared with matrix diffusion. This would in turn imply that the occurrence of some flow channelling may be a consisitent feature of the performed SWIW tests.

Table 5-3. Comparison of formation factor values measured in boreholes and calculated from estimated A values, respectively.

Borehole	Section (m)	F measured in borehole	F calculated from A p_m = 0.025
KSH02	422.3–423.3	6.3E–05	1.7E–03
KSH02	576.9–579.8	1.9E–04	1.3E–03
KLX03	740.4–744.4	4.4E–04	3.4E–02
KLX18A	473.3–476.3	Not available	3.2E–04
KLX11A	516.5–519.5	Not available	8.3E–02
KLX11A	598.0–599.0	Not available	2.2E–03
KFM02A	414.7–417.7	9.2E–05	3.33E–03
KFM03A	643.5–644.5	1.1E–04	3.51E–03
KFM08A	410.5–413.5	9.4E–05	2.29E–05
KFM04A	417.0–422.0	4.8E–04	Not evaluated
KFM01D	377.4–378.4	3.8E–05	8.49E–04
KFM01D	431.0–432.0	2.6E–05	1.55E–03

6 Summary and conclusions

This report presents a review of 12 SWIW tests performed within the SKB site investigations in Forsmark and Oskarshamn; six tests at each site have been carried out. The tests have been performed in surface boreholes at repository depth, ranging approximately between 300 to 700 m borehole lengths. An overall assessment is that experimental data appears to be of high quality, with smooth breakthrough curves without excessive noise and with well-documented experimental supporting data. Tracer recovery is generally high, although most of the tests are stopped before full recovery is obtained. However, it is indicated that full recovery is likely in all sections, except one, with sufficiently long recovery pumping.

In all of the SWIW tests, a non-sorbing (Uranine) and one or two sorbing tracers (Cs, Rb) have been injected simultaneously with the purpose of identifying retention effects for the sorbing tracers. A definite qualitative result is that more or less strong retardation effects for the sorbing tracers are clearly visible in the experimental breakthrough curves.

This report also presents evaluation of the SWIW tests with two simulation models. Both of the models are as simple as possible: 1) 1-D radial advection-dispersion with fracture retardation and 2) with added matrix diffusion and matrix retardation (but no fracture retardation). The first advection-dispersion model was employed as an initial basic model evaluation in connection with each test, in accordance with the SKB method description for SWIW tests (internal SKB document). The matrix diffusion model was employed as an extended evaluation and is presented in this report.

It is not assumed that either of the two models fully describes the transport geometry and acting transport processes, they are in fact very simple and highly idealized. However, employing models such as these may be a typical first approach for evaluating the performed SWIW tests. The evaluation results should also be valuable as a comparison for possible further evaluation with other interpretation approaches.

The basic evaluation with an advection-dispersion model (AD) was generally found to be sufficient to obtain a good fit of most of the experimental SWIW data. However, a consistent feature is that the tail of the breakthrough curve for the non-sorbing tracer (Uranine) can not be fitted with the AD-model and at the same time show a good fit of the rest of the curve. For the sorbing tracer(s), the fit was often relatively good to the entire breakthrough curve.

A number of possible effects caused by experimental equipment and procedures were considered in order to determine whether “artefacts” might be the reason for the observed tailing. However, it was not found likely that such effects would be the reason for the consistent tailing effect. Instead, it is considered more likely that the tailing is caused by other processes in the tested rock formation, such as diffusion into non-flowing parts of the tested rock feature.

The extended evaluation with the matrix diffusion model resulted in consistently improved fits for the tail of the Uranine curves, and in some cases also in improved fits for the sorbing tracers. Evaluated matrix diffusion parameters indicate relatively large diffusion effects, compared with literature data for matrix porosity and diffusivities. The interpreted matrix diffusion effect is of similar magnitude to cross-hole tracer tests evaluated with the same type of matrix diffusion model. The large diffusion effects may be an indication of diffusion into stagnant water adjacent to the flowing channels.

Evaluated retardation factors vary over a wide range, for both of the evaluation models. The relative magnitude among the various SWIW test sections is generally consistent between the two models. The interpreted differences in retardation likely reflect differences in rock characteristics and water chemistry. In some cases it may be possible to relate the test results

to observed fracture properties. For example, the tests in KFM02A showed a very low retardation compared with most other tests, which probably can be attributed to that there are no fracture minerals in any of the open fractures along the test section interval.

It is difficult to assess whether there are significant differences between sites regarding retardation, because the number of tests is limited. However, the largest values for the retardation factor are found for Oskarshamn and the smallest value in Forsmark. Moderate values in between are found at each site.

7 References

Altman S J, Meigs L C, Jones T L, McKenna S A, 2002. Controls of mass recovery rates in single-well injection-withdrawal tracer tests with a single-porosity, heterogeneous conceptualization, Water Resour. Res., 38(7), 1125, doi:10.1029/2000WR000182.

Andersson P, Gröhn S, Nordqvist R, Wass E, 2004. Aspö Hard Rock laboratory. TRUE block scale continuation project. BS2B pretests. Crosshole interference, dilution and tracer tests, CPT-1-CPT4. SKB IPR-04-25, Svensk Kärnbränslehantering AB.

Bear J, 1988. Dynamics of fluids in porous media. Dover Publications, Inc., New York.

Becker M W, Shapiro A M, 2003. Interpreting tracer breakthrough tailing from different forced-gradient tracer experiment configurations in fractured bedrock, Water Resour. Res., 39(1), 1024, doi:10.1029/2001WR001190.

Bodin J, Delay F, de Marsily G, 2003a. Solute transport in a single fracture with neglible matrix permeability: 1. Fundamental mechanisms. Hydrogeology Journal 11: 418–433.

Bodin J, Delay F, de Marsily G, 2003b. Solute transport in a single fracture with negligible matrix permeability: 2. Mathematical formalism. Hydrogeology Journal 11: 434–454.

Byegård J, Gustavsson E, Tullborg E-L, Selroos J-O, 2006a. Bedrock transport properties. Preliminary site desription Forsmark area – version 1.2. SKB R-05-86, Svensk Kärnbränslehantering AB.

Byegård J, Gustavsson E, Tullborg E-L, 2006b. Bedrock transport properties. Data evaluation and retardation model. Preliminary site desription Laxemar subarea – version 1.2. SKB R-06-27, Svensk Kärnbränslehantering AB.

Gelhar L W, Collins M A, 1971. General analysis of longitudinal dispersion in nonuniform flow. Water Resources Research, Vol 7., No. 6, pp 1511–1521.

Gustafsson E, 2002. Bestämning av grundvattenflödet med utspädningsteknik – Modifiering av utrustning och kompletterande mätningar. SKB R-02-31, Svensk Kärnbränslehantering AB (in Swedish).

Gustafsson E, Nordqvist R, Segerbäck D, Gröhn S, Olsson D, 2004. Site Acceptance Test (SAT) i borrhål KLX02 av Utspädningssond med SWIW-test utrustning (in Swedish). Geosigma GRAP 03085.

Gustafsson E, Nordqvist R, 2005. Oskarshamn site investigation. Ground water flow measurements and SWIW tests in borehole KLX02 and KSH02. SKB P-05-28, Svensk Kärnbränslehantering AB.

Gustafsson E, Nordqvist R, Thur P, 2005. Forsmark site investigation. Groundwater flow measurements in boreholes KFM01A, KFM02A, KFM03A, KFM03B and SWIW tests in KFM02A, KFM03A. SKB P-05-77, Svensk Kärnbränslehantering AB.

Gustafsson E, Nordqvist R, Thur P, 2006a. Oskarshamn site investigation. Groundwater flow measurements and SWIW test in borehole KLX03. SKB P-05-246, Svensk Kärnbränslehantering AB.

Gustafsson E, Nordqvist R, Thur P, 2006b. Forsmark site investigation. Groundwater flow measurements and SWIW test in borehole KFM08A. SKB P-06-90, Svensk Kärnbränslehantering AB.

Gustafsson E, Nordqvist R, Thur P, 2006c. Forsmark site investigation. Groundwater flow measurements and SWIW test in borehole KFM04A. SKB P-06-141, Svensk Kärnbränslehantering AB.

Haggerty R, Fleming S W, Meigs L C, McKenna S A, 2001. Tracer Tests in a Fractured Dolomite 2. Analysis of Mass Transfer in Single-Well Injection-Withdrawal Tests, Water Resour. Res., 37(5), 1129–1142.

Lessoff S C, Konikow L K, 1997. Ambiguity in measuring matrix diffusion with single-well injection/recovery tracer tests. Groundwater 35, no.1: 166–175.

Lindquist A, Hjerne C, Wass E, Byegård J, Nordqvist R, Walger E, Ludvigsson J-E, 2007. Forsmark site investigation. Confirmatory hydraulic interference test and tracer test at drillsite 2. Using sorbing and non-sorbing tracers. SKB report in prep, Svensk Kärnbränslehantering AB.

Liu J, Löfgren M, Neternieks I, 2006. SR-Can. Data and uncertainty assessment. Matrix diffusivity and porosity in situ. SKB R-06-111, Svensk Kärnbränslehantering AB.

Löfgren M, Neretnieks I, 2002. Formation factor logging in-situ by electrical methods. Background and methodology. SKB TR-02-27, Svensk Kärnbränslehantering AB.

Marquardt D W, 1963. An algorithm for least squares estimation of non-linear parameters. J. Soc. Ind. Appl. Math. 11:431–441.

de Marsily G, 1986. Quantitative hydrogeology. Academic Press, Inc.

Moreno L, Neretnieks I, Klockars C-E, 1983. Evaluation of some tracer tests in the granitic rock at Finnsjön. SKB TR 83-38, Svensk Kärnbränslehantering AB.

Neretnieks I, 2007. Single well injection withdrawal tests (SWIW) in fractured rock. Some aspects on interpretation. SKB R-07-54, Svensk Kärnbränslehantering AB.

Nordqvist R, Gustafsson E, 2002. Single-well injection-withdrawal tests (SWIW). Literature review and scooping calculations for homogenous crystalline bedrock conditions. SKB R-02-34, Svensk Kärnbränslehantering AB.

Nordqvist R, 2007. Extended evaluation of SWIW-tests in KSH02, a method study. SKB P-07-26, Svensk Kärnbränslehantering AB.

Ohlsson Y, Neretnieks I, 1995. Literature survey of matrix diffusion theory and of experiments and data including natural analogues. SKB TR 95-1, Svensk Kärnbränslehantering AB.

Thur P, Nordqvist R, Gustafsson E, 2007a. Oskarshamn site investigation. Groundwater flow measurements and SWIW tests in borehole KLX18A. SKB P-06-287, Svensk Kärnbränslehantering AB.

Thur P, Nordqvist R, Gustafsson E, 2007b. Forsmark site investigation. Groundwater flow measurements and SWIW tests in borehole KFM01D. SKB P-07-52, Svensk Kärnbränslehantering AB.

Thur P, Nordqvist R, Gustafsson E, 2007c. Oskarshamn site investigation. Groundwater flow measurements and SWIW tests in borehole KLX11A. SKB P-07-180, Svensk Kärnbränslehantering AB.

Voss C I, 1984. SUTRA – Saturated-Unsaturated Transport. A finite element simulation model for saturated-unsaturated fluid-density-dependent ground-water flow with energy transport or chemically-reactive single-species solute transport. U.S. Geological Survey Water-Resources Investigations Report 84-4369.